Transmission Lines Impedance Fitting Using Analytical Impedance Equation and Frequency Response Analysis

Hosam Alharbi [1] , Muhammad Khalid [2,3,4] and Mohammad Abido [2,3,5,*]

1   Electrical Engineering Department, Islamic University, Medina 42351, Saudi Arabia; 7071@iu.edu.sa
2   Electrical Engineering Department, King Fahd University of Petroleum and Minerals,
    Dhahran 31261, Saudi Arabia; mkhalid@kfupm.edu.sa
3   Interdisciplinary Research Center in Renewable Energy and Power Systems (IRC-REPS),
    King Fahd University of Petroleum and Minerals, Dhahran 31261, Saudi Arabia
4   Saudi Authority for Data and Artificial Intelligence-King Fahd University of Petroleum and Minerals Joint
    Research Center for Artificial Intelligence (SDAIA-KFUPM), Dhahran 31261, Saudi Arabia
5   K.A. CARE, Energy Research and Innovation Center (ERIC), King Fahd University of Petroleum and
    Minerals, Dhahran 31261, Saudi Arabia
*   Correspondence: mabido@kfupm.edu.sa; Tel.: +966-508757838

Abstract: Rational function approximation is commonly used to fit the transmission line impedance over a wide frequency range. Nevertheless, it is computationally costly and challenging to implement in practical applications due to the high number of approximations required to fit the impedance curve for the high-frequency range. Therefore, a novel fitting method of multiconductor transmission line (MTL) based on the analytical impedance equation of a transmission line using the impedance frequency response measurement is presented in this paper. The proposed fitting method is a function of the transmission line length since it is based on the analytical impedance equation of a finite transmission line. Furthermore, the proposed model uses a constant set of equations and calculated parameters to fit the impedance frequency response for a wide range of frequencies. Moreover, the proposed model parameters are calculated using derived resonance equations and the impedance frequency response measurement. In addition, an algorithm is developed to further fit the proposed model to the impedance frequency response measurement of the transmission line. MTL impedance frequency response is measured using a real-time digital simulator (RTDS). To ensure the accuracy of the proposed model, a comparison between the proposed model and vector fitting (VF) is presented.

1. Introduction

A transmission line is one of the major electrical components in a power system. Transmission lines are power guide components to deliver electric power from the source to the load. One of the key characteristic of a transmission line that differs from any electrical component is that transmission lines may cover long distances from the source to the load. Due to the length of a transmission line, a standing wave in a transmission line may occur. In addition, a wide range of different transient phenomena may affect transmission lines, such as lightning discharge, switching, and faults. Therefore, developing an accurate model of a transmission line is essential to predict the behavior of transmission lines in different transient scenarios.

Vector Fitting (VF) is a general methodology used to fit the measured or simulated transient frequency response of electric equipment or an n-port network. VF uses a rational

function approximation method to fit measured data to the rational function [1]. In [2–4], the authors presented a transient model of multiconductor transmission line (MTL) using VF. In [5], a hybrid phase domain transmission line transient model is introduced, which utilizes the transpose of a transmission line to have a lower computational time without loss of accuracy. VF has been used in time domain modeling as well as frequency-domain modeling of a transmission line. In [6], time-domain modeling of partial discharge on medium voltage cables using the VF Method is presented. The proposed model in [6] uses the VF method to incorporate the skin effects and dielectric losses into the state matrices. In [7], a fast realization of the modal VF method (MVF) is presented. MVF has a faster pole and residue identification step and a lower number of iterations required to obtain the state-space model. In [8], a frequency-dependent cable model (FDCM) is presented, which solves an issue associated with the eigenvalues by reducing the rank of the propagation matrix to obtain a smooth fitting model.

Some research papers focus more on the low-frequency range or DC transient modeling. In [9], an enhanced fitting technique for the transient response of the transmission line is presented. The proposed model uses low-order fitting of a function error for every line parameter to obtain an accurate DC transient model of transmission lines. Moreover, a frequency domain transient transmission line model is presented in [10], which emphasizes the low-frequency transient response. The presented transient model in [10] consists of two-stage, low-frequency, and high-frequency models. In addition, the authors in [10] focus on minimizing the error of a curve fitting for the low-frequency range due to the instability of the poles at low-frequency.

Many papers address a specific transient phenomenon to be integrated into the transient modeling of transmission lines. Gunawardana and Kordi, in [11], address the issue of the transient behavior of transmission lines crossing. The developed model utilizes the electromagnetic scattering theory to calculate space varying per unit length (PUL) parameter matrices close to the conductor crossing. The presented model in [11] considers different crossing angles for lossless and frequency-independent transmission lines. In [12], accurate transient modeling of skin effect of MTL is proposed, where the authors take into account the transient behavior of transmission line skin effects.

In addition to the frequency domains model, many different time-domain models have been presented in the research. For instance, in [13], a transient model of MTLs using the Time-Domain Finite-Element (TDFE) method is presented. The proposed model in [13] is used for loose MTLs with frequency-dependent parameters to simulate the transient behavior of MTLs. In addition, a real-time optimized transient modeling of a transmission line is presented in [14], where the developed method subdivided the transmission line modeling (TLM) into individual nonlinear elements to reduce the simulation time. Moreover, a time-domain model of multiphase nonuniform lines (NULs) is introduced in [15], where the proposed model is based on traveling waves and takes into account the frequency dependence of the line parameters. In [16], a time-domain macromodeling method for the transient responses of underground cables is presented. The frequency-dependent variables are modeled using frequency response and then converted to the time domain transient model.

An estimation algorithm for mutually coupled transmission line parameters is developed in [17]. The presented model deals with the mutually coupled transmission line as a black box and measures the voltages and the currents at the sending end during a transient event. Then, the proposed algorithm obtains the unknown transmission line parameters during the transient event from the measured voltages and currents. In [18], frequency-dependent line model is developed, which utilizes the concept of frequency-adaptive simulation of transients in which the Fourier spectra are adaptively shifted in the frequency domain to reduce the discretization time-steps in the time domain. In [19], a new Frequency-Dependent Line Model (FDLM) is proposed based on the Revised Multiconductor Transmission Line (RMTL) equations. The proposed model postulated the physical constraint that the voltage and current waves should travel collocated.

Transmission line impedance fitting commonly uses a rational function approximation to fit the model to the measurements. VF is a well-known and developed rational approximation function used in transmission line impedance fitting. Table 1 shows some of the advantages and disadvantages of the VF method. VF is not a function in transmission line length. Therefore, changing the length of the transmission line will require retaking the impedance frequency response of the transmission line and developing a new model for the transmission line. In contrast, the proposed model is developed based on the analytical impedance equation of finite transmission lines. Therefore, the proposed model will not require retaking the impedance frequency response and developing a new model. VF method obtains a two ports system for a transmission line. Therefore, changing the frequency range of the impedance frequency response will require developing a new model. In contrast, the proposed model is developed based on the transmission line lumped model. Thus, the proposed model will remain the same for a wide range of frequencies with a low error between the measurement and the fitted impedance. VF method uses a rational function to fit the impedance frequency response as-is. Therefore, a low sampling rate in the high-frequency range, even though fitted to a high degree of accuracy, will not give an accurate representation of the transmission line impedance. On the other hand, the presented model in this paper uses the transmission line impedance equation to fit the impedance frequency response. Therefore, the proposed model will give a better representation of the impedance frequency response, even with a lower sampling rate for a high-frequency range.

Table 1. Vector fitting method advantages and disadvantages.

Advantages	Disadvantages
VF model can be used in time domain and frequency domain.	The rational function approximation is not a function in the transmission line length.
VF Capable of fitting the impedance to a high degree of accuracy.	The rational function approximation is a mathematical function that is not correlated to the impedance of the transmission line. Thus, it fits the data as-is.
VF enforces passivity to obtain a passive model.	VF required high computation power to obtain the model.
VF is a general mathematical model capable of fitting any physical quantity with an amplitude and angle (Vector).	The obtained model changes with the frequency range.

This paper presents a novel fitting method of MTL based on the analytical impedance equation of a transmission line using the impedance frequency response measurement. To test the accuracy of the proposed model, a comparison between the proposed model and a well-known and developed VF is presented. The impedance frequency response of transmission lines is measured using a real-time digital simulator (RTDS).

The main contributions of the article are:

- Develop a fitting method for MTL impedance based on the analytical impedance equation. This will ensure that the proposed method behaves similarly to the transmission line impedance.
- Develop a fitting method for MTL impedance which is a function of transmission line length. This is to ensure that the proposed model will have an accurate representation of the transmission line impedance for different transmission line lengths.
- Develop a fitting method capable of fitting MTL impedance for a wide range of frequencies without modifying the model for higher frequencies.

Section 2 shows the basic fundamentals on which the rest of the research is based on. Section 3 presents how the measurement of impedance frequency response is conducted and the transmission line data. In addition, a comparison between a single-phase and MTL measurement is presented. Moreover, the proposed model for MTL impedance fitting

equation is presented as the reason for selecting the proposed model as well. Section 4 presents the deviation of resonance equations from the proposed model and how the parameters of the proposed model are calculated from the impedance frequency response and derived equations. In addition, a comparison between the measured impedance frequency response and fitted impedance based on the model parameters calculation is presented. Section 5 presents a developed algorithm used to improve the impedance fitting of the proposed model and the impedance frequency response measurement. In addition, Section 5 shows the error between the calculated parameters and the fitted parameters. Section 6 presents the simulation and results. Section 7 details the features of the proposed model over rational function approximation. Section 8 concludes the paper.

2. Wave Characteristics on Finite Transmission Lines

The wave characteristics of finite transmission lines impedance are determined by the impedance equation of the transmission line. The impedance of the transmission line is given by [20]:

$$Z = Z_0 \frac{Z_L + Z_0 \times \tanh{(\gamma l)}}{Z_0 + Z_L \times \tanh{(\gamma l)}} \tag{1}$$

For short-circuit transmission line where the load impedance $Z_L = 0$:

$$Z = Z_0 \times \tanh{(\gamma l)} \tag{2}$$

where the characteristic impedance of the line is given by:

$$Z_0 = \sqrt{\frac{R + j\omega L}{G + j\omega C}} \tag{3}$$

and, the propagation constant is given by:

$$\gamma = \alpha + j\beta = \sqrt{(R + j\omega L)(G + j\omega C)} \tag{4}$$

where:

- α, attenuation constant, in Np/m.
- β, phase constant, in rad/m.
- R, resistance per unit length, in Ω/m.
- L, inductance per unit length, in H/m.
- G, conductance per unit length, in S/m.
- C, capacitance per unit length, in F/m.
- l, length of the transmission line, in m.

For lossless transmission line:

$$Z_0 = R_0 = \sqrt{\frac{L}{C}} \tag{5}$$

$$\gamma = j\beta = j\omega\sqrt{LC} \tag{6}$$

$$\tanh{(\gamma l)} = \tanh{(j\beta l)} = j\tan{(\beta l)} \tag{7}$$

Therefore, the impedance of a lossless short-circuited transmission line is given by ($Z_L = 0$):

$$Z = jR_0 \tan{(\beta l)} \tag{8}$$

Figure 1 shows the impedance frequency response of short-circuited transmission line as described by (8). The impedance of short-circuited transmission line oscillates between inductive and capacitive depending on the value of βl, which is frequency dependent, see Table 2.
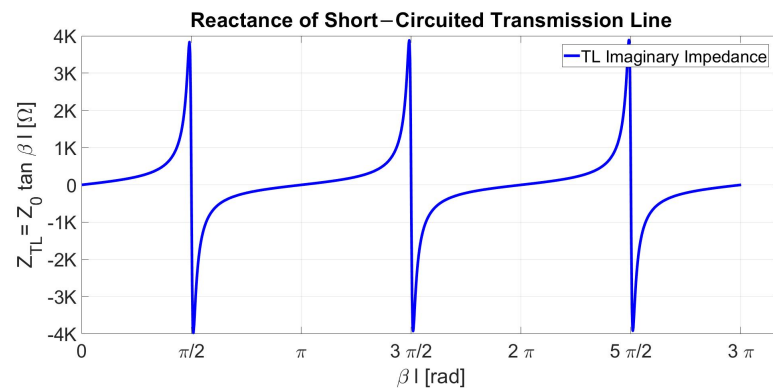
Figure 1. Reactance profile of Short–Circuited lossless Line [20].

Table 2. Reactance range of Short–Circuited lossless Line [20].

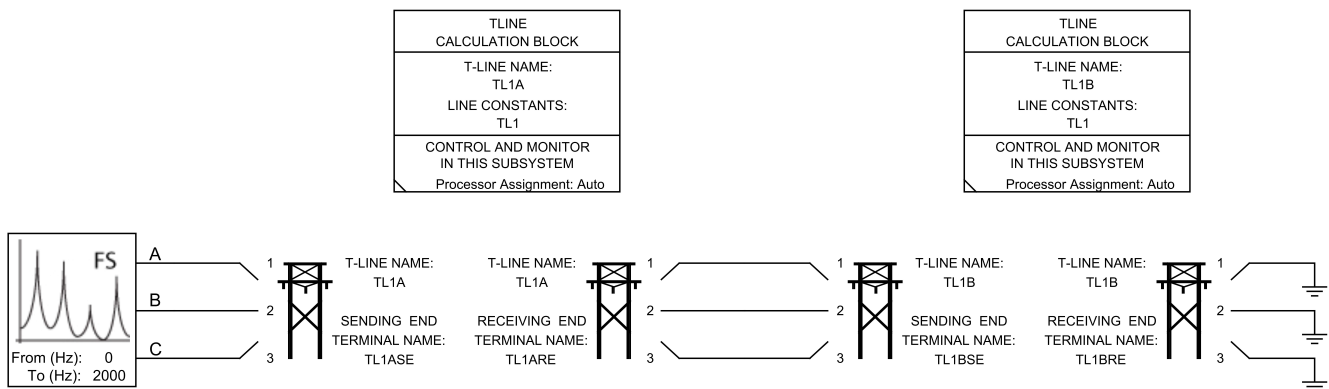| l	βl	Z_{TL}
$(n-1)\frac{\lambda}{2} < l < (2n-1)\frac{\lambda}{4}$	$(n-1)\frac{\pi}{4} < \beta l < (2n-1)\frac{\pi}{2}$	Inductive
$(2n-1)\frac{\lambda}{4} < l < n\frac{\lambda}{2}$	$(2n-1)\frac{\pi}{2} < \beta l < n\pi$	Capacitive
$n\frac{\lambda}{2}$	$n\pi$	0
where $n = 1, 2, 3, \ldots$		

3. The Frequency Response of Transmission Lines Impedance and the Proposed Model of MTL

In the previous section, the impedance frequency response of short-circuited transmission line has been shown using the analytical solution, see (8). Frequency Response Analysis (FRA) is a methodology used to measure the frequency response of an impedance function or a transfer function. A similar tool in RTDS called frequency scan "_rtds_FREQSCAN" is used to obtain the impedance frequency response of short-circuited transmission line over a wide range of frequencies. The frequency scan has a maximum range of 1MHz. The frequency scan output a text file containing all the impedance matrices at their measured frequencies. Therefore, RTDS is used to obtain the FRA impedance measurements of a short-circuited transmission line. The data of the transmission line, which will be modeled and studied, is shown in Table 3. Figure 2 shows the circuit diagram of FRA measurement in RTDS.

Table 3. Transmission line Bergeron model parameters.

| Model	Bergeron (RLC Data Entry)
Line Length	100 [Km]
Transposition	Ideally Transposed
Frequency	60 [Hz]
Ground Resistivity	100 [Ω- m]
Number of Phases	3
Positive Sequence Series Resistance	0.018547 [Ω/Km]
Positive Sequence Series Ind. Reactance	0.37661 [Ω/Km]
Positive Sequence Shunt Cap. Reactance	0.22789 [MeagaΩ× Km]
Zero Sequence Series Resistance	0.3618376[Ω/Km]
Zero Sequence Series Ind. Reactance	1.227747 [Ω/Km]
Zero Sequence Shunt Cap. Reactance	0.34513 [MeagaΩ× Km]

**Figure 2.** RTDS circuit Line Diagram of FRA measurements.

The FRA measurements of transmission line impedance are obtained in a symmetrical matrix format from RTDS. The impedance matrix of the transmission line at every measured frequency point is in the form of:

$$\begin{bmatrix} Z_{11} & Z_{12} & Z_{13} \\ Z_{21} & Z_{22} & Z_{23} \\ Z_{31} & Z_{32} & Z_{33} \end{bmatrix} \tag{9}$$

The impedance matrices of the transmission line are measured at different frequency points in a defined frequency range. To obtain a higher sampling rate and present clear graphs, the shown measurements were taken up to 2 kHz with 200 k samplings. The imaginary and real values of the transmission line impedance measurements of Z_{11} are shown in Figures 3 and 4, respectively.
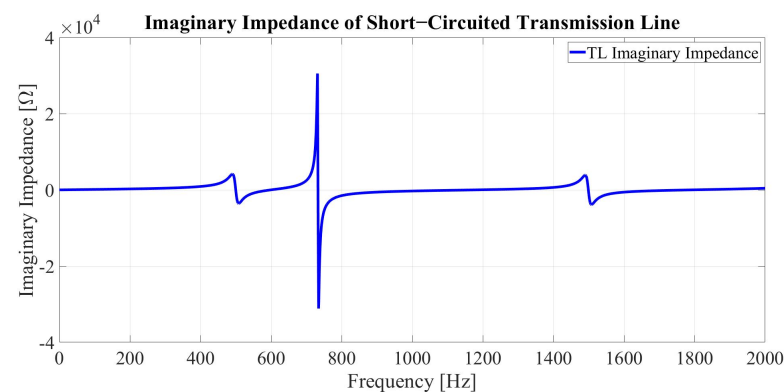
Figure 3. Frequency response measurements of transmission line imaginary impedance.
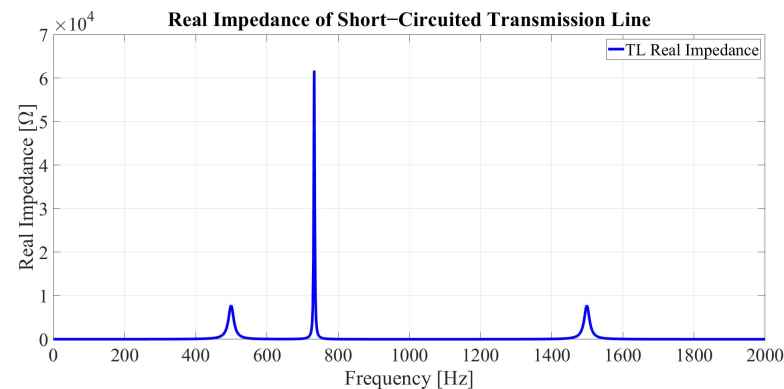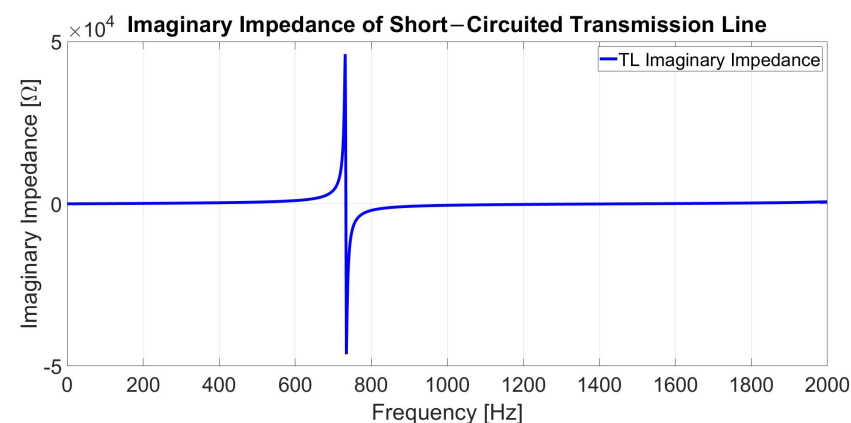

Figure 4. Frequency response measurements of transmission line real impedance.

Figure 3 shows sharp changes in the imaginary part of the transmission line impedance from maximum positive to minimum negative values (inductive to capacitive) at $f_{o1} = 500$ Hz and at $f_{o2} = 733$ Hz, and slower changes from capacitive to inductive at 600 Hz and at 1200 Hz. Since the sharp changes from inductive to capacitive or vice versa (f_{o1} and f_{o2}) are associated with high real impedance values, then it will be considered as the resonance frequency of the transmission line. By analyzing Figures 3 and 4, we can see that the resonance frequencies take place when the imaginary part of the transmission line impedance is equal to zero, and the real part of the transmission line impedance is at maximum. Moreover, Figure 3 shows two sets of resonance frequencies, while Figure 5 shows only one resonance. This is because (2) is for a single-phase transmission line, while FRA impedance measurement shown in Figures 3 and 4 are for MTLs. Therefore, by changing the number of phases to one and maintaining the same parameters, see Table 4, a single resonance of a single-phase transmission line resonance will appear as shown in Figures 5 and 6.

Table 4. Transmission line Bergeron model parameters.

Model	Bergeron (RLC Data Entry)
Line Length	100 [Km]
Frequency	60 [Hz]
Ground Resistivity	100 [Ω-m]
Number of Phases	1
Positive Sequence Series Resistance	0.018547 [Ω/Km]
Positive Sequence Series Ind. Reactance	0.37661 [Ω/Km]
Positive Sequence Shunt Cap. Reactance	0.22789 [MeagaΩ× Km]

Figure 5. Frequency response measurements of a single phase transmission line imaginary impedance.
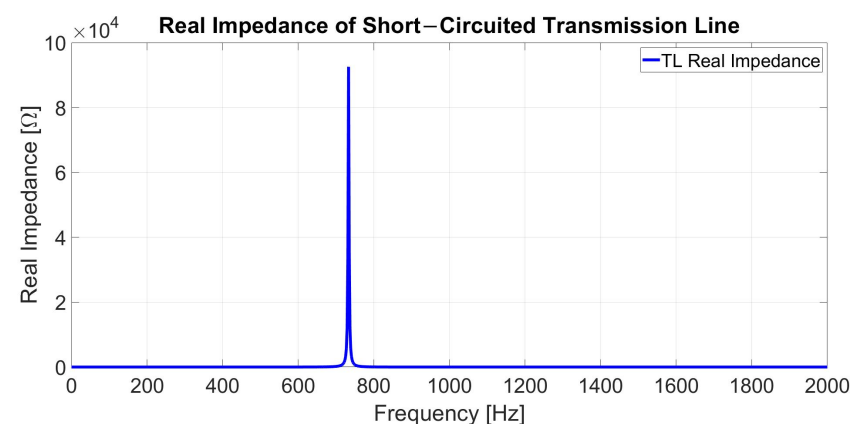
Figure 6. Frequency response measurements of a single phase transmission line real impedance.

Therefore, due to the mutual coupling between the phases, a second resonance appears in addition to the first resonance of a single transmission line. Moreover, both resonances have the same repeated pattern $(2n + 1) \times f_0$, which is associated with the tanh function. Therefore, a more accurate representation of the MTL impedance equation (in the case Z_{11}) is proposed to be:

$$Z_{11} = Z_{o1} \times \tanh \gamma_1 l + Z_{o2} \times \tanh \gamma_2 l \tag{10}$$

let

$$Z_1 = Z_{o1} \times \tanh \gamma_1 l \tag{11}$$

$$Z_2 = Z_{o2} \times \tanh \gamma_2 l \tag{12}$$

where Z_1 represents the lumped mutual coupling impedance of the transmission line and Z_2 represents the lumped self impedance of the transmission line. Equation (10) will be used to model the MTLs impedance instead of (2). The added second term in (10) is because the frequency response of MTLs impedance (for Z_{11}) has a second resonance, and due to the similarity and nature of both resonances, the same function (tanh) is used. In the next section, the parameters of the proposed model (10) will be calculated using derived resonance equations and the impedance frequency response of MTL.

4. Parameters of MTLs Proposed Impedance Equation

To obtain the parameters of the proposed transmission line impedance equation (in this case for Z_{11}), a set of equations must be derived from the complex nonlinear transmission line impedance equation:

$$Z_{11} = Z_1 + Z_2 \tag{13}$$

$$Z_{11} = Z_{o1} \times \tanh \gamma_1 l + Z_{o2} \times \tanh \gamma_2 l \tag{14}$$

where

$$Z_{o1} = \sqrt{\frac{R_1 + j\omega L_1}{G_1 + j\omega C_1}} \qquad\qquad Z_{o2} = \sqrt{\frac{R_2 + j\omega L_2}{G_2 + j\omega C_2}} \tag{15}$$

$$\gamma_1 l = \sqrt{(R_1 + j\omega L_1)(G_1 + j\omega C_1)} \tag{16}$$

$$\gamma_2 l = \sqrt{(R_2 + j\omega L_2)(G_2 + j\omega C_2)} \tag{17}$$

The transmission line length is multiplied by the per unit length parameters. Thus, the parameters shown are for the entire length of the transmission line. Therefore, the transmission line impedance of Z_{11}:

$$Z_{11} = \sqrt{\frac{R_1 + j\omega L_1}{G_1 + j\omega C_1}} \times \tanh \sqrt{(R_1 + j\omega L_1)(G_1 + j\omega C_1)} + \sqrt{\frac{R_2 + j\omega L_2}{G_2 + j\omega C_2}} \times \tanh \sqrt{(R_2 + j\omega L_2)(G_2 + j\omega C_2)} \tag{18}$$

Since the air resistance between phases and between phase and ground is very high ($10^9 \frac{\Omega}{m}$), then let:

$$G_1 = G_2 = 10^{-9} \tag{19}$$

Since the capacitance in μF and the measured impedance frequency range is 10^{-6} Hz to 2 MHz, then at low-frequency

$$\tanh \sqrt{(R_1 + j\omega L_1)(G_1 + j\omega C_1)} = \sqrt{(R_1 + j\omega L_1)(G_1 + j\omega C_1)} \tag{20}$$

$$\tanh \sqrt{(R_2 + j\omega L_2)(G_2 + j\omega C_2)} = \sqrt{(R_2 + j\omega L_2)(G_2 + j\omega C_2)} \tag{21}$$

Therefore, (18) at low-frequency will be:

$$R_1 + R_2 + j\omega(L_1 + L_2) = Z_{11} \tag{22}$$

Let,

$$R_T = R_1 + R_2 \qquad\qquad L_T = L_1 + L_2 \qquad (23)$$

where

$$R_T = Real(Z_{11})_{at10^{-6}Hz} \qquad (24)$$

$$L_T = \frac{Im(Z_{11})_{at10^{-6}Hz}}{\omega} \qquad (25)$$

where R_T and L_T are the total resistance and inductance, respectively, obtained from transmission line FRA measurement at 10^{-6} Hz. Figure 7 shows two resonances ($f_{01} = 500$ and $f_{02} = 733$) where the imaginary part of the transmission line impedance equals zero, and the real part is at maximum. Moreover, Figure 7 shows two distinct maximum values of the real part. Each one of them is associated with a term in (18). Therefore, Equation (18) must be written in rectangular complex format (real and imaginary) to obtain the transmission line parameters. From equating the imaginary part of (18) to zero and the real part by the relative maximum values, a set of equations must be derived first. The derivation of the resonance equations will be presented in the next section.
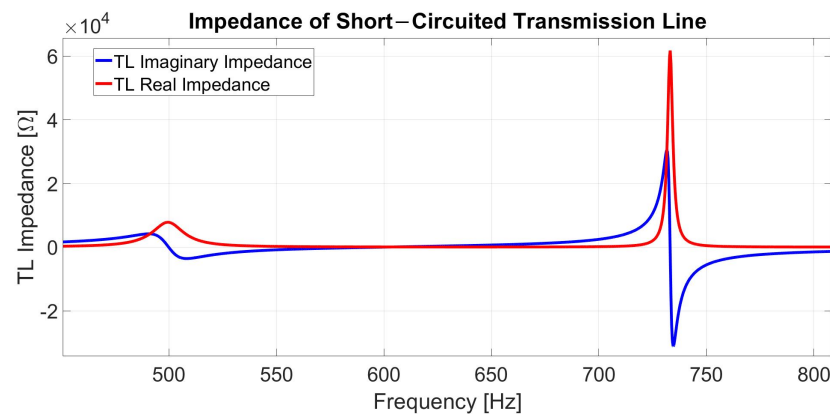
Figure 7. Frequency response measurements of transmission line impedance.

4.1. Derivation of Resonance Equations

To obtain the parameters of the proposed transmission line impedance equation (in this case for Z_{11}), a set of equations must be derived from the complex nonlinear transmission line impedance equation at the resonance, ($f_{01} = 500$ and $f_{02} = 733$). Since the imaginary part of Z_{11} equals to zero at resonance ($f_{01} = 500$ and $f_{02} = 733$) then,

$$Im(\sqrt{\frac{R_1 + j\omega L_1}{G_1 + j\omega C_1}} \times \tanh \sqrt{(R_1 + j\omega L_1)(G_1 + j\omega C_1)} + \sqrt{\frac{R_2 + j\omega L_2}{G_2 + j\omega C_2}} \times \tanh \sqrt{(R_2 + j\omega L_2)(G_2 + j\omega C_2)}) = 0 \qquad (26)$$

First we take the first part of (26),

$$Im(\sqrt{\frac{R_1 + j\omega L_1}{G_1 + j\omega C_1}} \times \tanh \sqrt{(R_1 + j\omega L_1)(G_1 + j\omega C_1)}) \qquad (27)$$

let,

$$\gamma_1 = \sqrt{(R_1 + j\omega L_1)(G_1 + j\omega C_1)} \qquad (28)$$

Using De Moivre's theorem:

$$r = \sqrt{\sqrt{(R_1 G_1 - \omega^2 L_1 C_1)^2 + (\omega L_1 G_1 + \omega C_1 R_1)^2}} \qquad (29)$$

$$\theta = \frac{1}{2} \tan^{-1}\left(\frac{\omega L_1 G_1 + \omega C_1 R_1}{R_1 G_1 - \omega^2 L_1 C_1}\right) \tag{30}$$

Therefore,

$$\gamma_1 = -r \sin\theta + i r \cos\theta \tag{31}$$

Similarly

$$Z_{01} = \sqrt{\frac{R_1 + j\omega L_1}{G_1 + j\omega C_1}} = \sqrt{\frac{(R_1 + j\omega L_1)(G_1 + j\omega C_1)}{(G_1 + j\omega C_1)(G_1 + j\omega C_1)}} \tag{32}$$

Let

$$A = \frac{1}{G_1^2 + \omega^2 C_1^2} \tag{33}$$

Then

$$Z_{01} = (-AG_1 r \sin\theta + \omega AC_1 r \cos\theta) + i(AG_1 r \cos\theta + \omega AC_1 r \sin\theta) \tag{34}$$

Let

$$h = (-AG_1 r \sin\theta + \omega AC_1 r \cos\theta) \tag{35}$$

$$k = (AG_1 r \cos\theta + \omega AC_1 r \sin\theta) \tag{36}$$

$$a = -r \sin\theta \qquad\qquad b = r \cos\theta \tag{37}$$

Then

$$Z_{01} = h + i k \qquad\qquad \gamma_1 = a + i b \tag{38}$$

Therefore

$$Z_1 = (h + i k) \tanh(a + i b) \tag{39}$$

Since

$$\tanh(x) = \frac{e^x - e^{-x}}{e^x + e^{-x}} \tag{40}$$

$$Z_1 = (h + i k)\frac{e^{a+ib} - e^{-a-ib}}{e^{a+ib} + e^{-a-ib}} \tag{41}$$

Solving for the numerator first

$$Z_1 = (h + i k)(e^a e^{ib} - e^{-a} e^{-ib}) \tag{42}$$

Let

$$A_1 = e^a \qquad\qquad A_2 = e^{-a} \tag{43}$$

Then

$$Z_1 = (h + i k)[(A_1 - A_2)\cos b + i(A_1 + A_2)\sin b] \tag{44}$$

Let

$$x = (A_1 - A_2)\cos b \qquad\qquad y = (A_1 + A_2)\sin b \tag{45}$$

Therefore,

$$Z_1 = (hx - ky) + i(hy + kx) \tag{46}$$

$$hy + kx = AG_1 r A_1 \cos(\theta + b) - AG_1 r A_2 \cos(\theta - b) + \omega AC_1 r A_1 \sin(\theta + b) - \omega AC_1 r A_2 \sin(\theta - b) \tag{47}$$

$$hx - ky = -AG_1rA_1 \sin(\theta + b) + AG_1rA_2 \sin(\theta - b) + \\ \omega AC_1rA_1 \cos(\theta + b) - \omega AC_1rA_2 \cos(\theta - b)$$ (48)

Let the real parts of the equation equal to:

$$A_5 = AG_1r(A_2 \sin(\theta - b) - A_1 \sin(\theta + b))$$ (49)

$$A_6 = \omega AC_1r(A_1 \cos(\theta + b) - A_2 \cos(\theta - b))$$ (50)

Let the imaginary parts of the equation equals to:

$$A_7 = AG_1r(A_1 \cos(\theta + b) - A_2 \cos(\theta - b))$$ (51)

$$A_8 = \omega AC_1r(A_1 \sin(\theta + b) - A_2 \sin(\theta - b))$$ (52)

Let,

$$\gamma = \theta - b \qquad\qquad \beta = \theta + b$$ (53)

For the denominator

$$e^{a+ib} + e^{-a-ib} = A_1 \cos b + A_2 \cos b + i(A_1 \sin b - A_2 \sin b)$$ (54)

Multiplying by the complex conjugate, the denominator will be

$$D = [(A_1 + A_2) \cos b]^2 + [(A_1 - A_2) \sin b]^2$$ (55)

Multiplying the numerators (Equations (49)–(52)) by the complex conjugate of the denominator:

$$A_1 \cos b + A_2 \cos b - i(A_1 \sin b - A_2 \sin b)$$ (56)

We get:

$$Real_{11} = AG_1r(A_1^2 \sin(-\theta) - A_1A_2 \sin(\theta + 2b) + \\ A_1A_2 \sin(\theta - 2b) + A_2^2 \sin(\theta))$$ (57)

$$Real_{22} = \omega AC_1r(A_1^2 \cos(-\theta) - A_2A_1 \cos(\theta - 2b) + \\ A_1A_2 \cos(\theta + 2b) - A_2^2 \cos(\theta))$$ (58)

Therefore

$$Real(Z_1) = \frac{Real_{22} + Real_{11}}{D}$$ (59)

For the imaginary part:

$$Im_{11} = AG_1r(A_1^2 \cos(-\theta) - A_2A_1 \cos(\theta - 2b) + \\ A_1A_2 \cos(\theta + 2b) - A_2^2 \cos(\theta))$$ (60)

$$Im_{22} = \omega AC_1r(A_1^2 \sin(\theta) - A_2A_1 \sin(\theta - 2b) + \\ A_1A_2 \sin(\theta + 2b) - A_2^2 \sin(\theta))$$ (61)

$$Im(Z_1) = \frac{Im_{22} + Im_{11}}{D}$$ (62)

$$Z_1 = Z_{o1} \times \tanh \gamma_1 l = \frac{Real_{22} + Real_{11}}{D} + j\frac{Im_{22} + Im_{11}}{D}$$ (63)

Similarly, for the second part of (26):

$$Z_2 = Z_{o2} \times \tanh \gamma_2 l = \frac{Real_{33} + Real_{44}}{D_1} + j\frac{Im_{33} + Im_{44}}{D_1}$$ (64)

At the resonance frequency the imaginary value goes to zero while the real value will be at maximum, therefore:

$$\frac{Im_{22} + Im_{11}}{D} + \frac{Im_{33} + Im_{44}}{D_1} = 0 \tag{65}$$

Since Im_{11} and Im_{33} is multiplied by G_1 and G_2, respectively (where both are equal to 10^{-9}), then (65) will be:

$$Im_{22}D_1 + Im_{44}D = 0 \tag{66}$$

Since $\omega AC_1 r D_1$ cannot be zero, then

$$A_1^2 \sin(\theta) - A_2 A_1 \sin(\theta - 2b) + A_1 A_2 \sin(\theta + 2b) - A_2^2 \sin(\theta) = 0 \tag{67}$$

To make (67) equal to zero then,

$$\theta = 0 \qquad\qquad b = \frac{\pi}{2} \tag{68}$$

One characteristic of the transmission line imaginary impedance is the sharp change at resonance; this is due to the tanh function. Solving for a single-phase transmission line impedance will result in Im_{22} equals to zero at resonance. Therefore, by adding a second term $Im_{44}D$, the resonance frequency will increase or decrease by a small value due to the sharp change at resonance. In addition, the peak to peak value of the first term of (66) at the first resonance compared to the impedance of the second term is very high. The second characteristic is that the resonance of both terms is repeated according to $(2n + 1)$ since it is a tanh function. Therefore, the two resonances will come close and separate apart at different frequency points through the frequency range. Therefore, the effects of the second resonance on the first resonance will change through the frequency range. Thus, taking the measurement of the resonance location with minimum effects from the second resonance will give an accurate result. This will not affect the derived equations but will emphasize the impact of the selected measurement throughout the frequency range. Therefore, the second part of (66) is forced to be zero, assuming no effects on the first resonance. Since

$$b = r \, \cos(\theta) = \frac{\pi}{2} \tag{69}$$

Then,

$$r = \sqrt{\sqrt{(R_1 G_1 - \omega^2 L_1 C_1)^2 + (\omega L_1 G_1 + \omega C_1 R_1)^2}} = \frac{\pi}{2} \tag{70}$$

$$L_1^2 = \frac{\frac{\pi^4}{16} - \omega^2 C_1^2 R_1^2 - R_1^2 G_1^2}{\omega^4 C_1^2 + \omega^2 G_1^2} \tag{71}$$

Since G_1 has a very small value, then:

$$L_1^2 = \frac{\frac{\pi^4}{16} - \omega^2 C_1^2 R_1^2}{\omega^4 C_1^2} \tag{72}$$

Since the value of C is in μF, and the first resonance takes place under 1 kHz, then

$$\frac{\pi^4}{16} >> \omega^2 C_1^2 R_1^2 \tag{73}$$

Then

$$L_1^2 \omega^4 C_1^2 = \frac{\pi^4}{16} \tag{74}$$

$$\frac{\pi^2}{4\omega^2} = L_1 C_1 \tag{75}$$

Similarly, for the second resonance:

$$\frac{\pi^2}{4\omega_2^2} = L_2 C_2 \tag{76}$$

Solving for the real part, we can ignore the real part associated with Z_2 to solve for Z_1 and vice versa. This is due to the high real part impedance value of Z_1 at resonance (f_{o1}) compared to the real value of Z_2 at f_{o1}. Since the real part of Z_1 will equal to a maximum at f_{01} when θ equals zero and b equals to $\pi/2$, then

$$Real(Z_1) = \frac{Real_{22} + Real_{11}}{D} \tag{77}$$

Since $Real_{11}$ is multiplied by G_1, then

$$Real_{11} \approx 0 \tag{78}$$

Since θ equals zero and b equals to $\pi/2$

$$Real_{22} = \omega A C_1 r (A_1^2 \cos(-\theta) - A_2 A_1 \cos(\theta - 2b) + \tag{79}$$
$$A_1 A_2 \cos(\theta + 2b) - A_2^2 \cos(\theta))$$

Then

$$Real_{22} = \omega A C_1 r (A_1^2 - A_2^2) \tag{80}$$

Since

$$D = (A_1 - A_2)^2 \tag{81}$$

Let the maximum impedance of the real part be equal to:

$$Real(Z_1) = Z_{R1} \tag{82}$$

Then

$$Z_{R1} = \omega A C_1 r \frac{(A_1^2 - A_2^2)}{(A_1 - A_2)^2} \tag{83}$$

$$Z_{R1} = \omega A C_1 r \frac{(A_1^2 - A_2^2)}{(A_1^2 + A_2^2 - 2)} \tag{84}$$

$$Z_{R1} = \omega A C_1 r \frac{e^{-2r\sin(\theta)} - e^{2r\sin(\theta)}}{e^{-2r\sin(\theta)} + e^{2r\sin(\theta)} - 2} \tag{85}$$

Since

$$-\coth(\frac{1}{2}x) = \frac{e^{-x} - e^x}{e^{-x} + e^x - 2} \tag{86}$$

Then,

$$Z_{R1} = -\omega A C_1 r \, \coth(\frac{1}{2} 2r \sin(\theta)) \tag{87}$$

$$\coth(x) = \frac{\cosh(x)}{\sinh(x)} \tag{88}$$

Since the angle θ is very small at resonance, then,

$$\cosh(x) = 1 \qquad\qquad \sinh(x) = x \tag{89}$$

Therefore

$$Z_{R1} = \omega A C_1 r \frac{1}{r \sin(\theta)} \tag{90}$$

Since

$$A = \frac{1}{G_1^2 + \omega^2 C_1^2} \tag{91}$$

And the values of G_1 and θ are small, then

$$Z_{R1} = -\frac{1}{\omega C} \frac{1}{\theta} \tag{92}$$

where,

$$\theta = \frac{1}{2} \tan^{-1} \left(\frac{\omega L_1 G_1 + \omega C_1 R_1}{R_1 G_1 - \omega^2 L_1 C_1} \right) \tag{93}$$

Initially the value of θ made to equal zero to solve for the imaginary part. Substituting θ by zero in (92) will result in infinity. The impedance value during resonance is high but not infinite. In addition, Equation (93) can not equal zero due to the summation of two positive number in the numerator, thus the value of θ should be small (close to zero). Since G_1 has a small value as well as $\left(\frac{\omega L_1 G_1 + \omega C_1 R_1}{R_1 G_1 - \omega^2 L_1 C_1} \right)$ at resonance, then

$$\theta = \frac{1}{2} \left(\frac{\omega C_1 R_1}{-\omega^2 L_1 C_1} \right) \tag{94}$$

$$\theta = \frac{R_1}{-2\omega L_1} \tag{95}$$

Therefore, the real part of the impedance at the crossover frequency will be:

$$Z_{R1} = \frac{2L_1}{C_1 R_1} \tag{96}$$

Similarly for the second resonance,

$$Z_{R2} = \frac{2L_2}{C_2 R_2} \tag{97}$$

Therefore, the derived resonance equations are:

$$\boxed{L_1 C_1 = \frac{\pi^2}{4\omega_1^2}} \qquad \boxed{L_2 C_2 = \frac{\pi^2}{4\omega_2^2}} \tag{98}$$

$$\boxed{Z_{R1} = \frac{2L_1}{C_1 R_1}} \qquad \boxed{Z_{R2} = \frac{2L_2}{C_2 R_2}} \tag{99}$$

where:
Z_{R1}: is the maximum peak of the real part of the transmission line impedance at f_{o1}.
Z_{R2}: is the maximum peak of the real part of the transmission line impedance at f_{o2}.
Equation (99) and Figure 8 show that the maximum real impedance of transmission line (Z_{R1}) and (Z_{R2}) at resonance is dependent on transmission line parameters (R, L, and C) and not on the frequency.
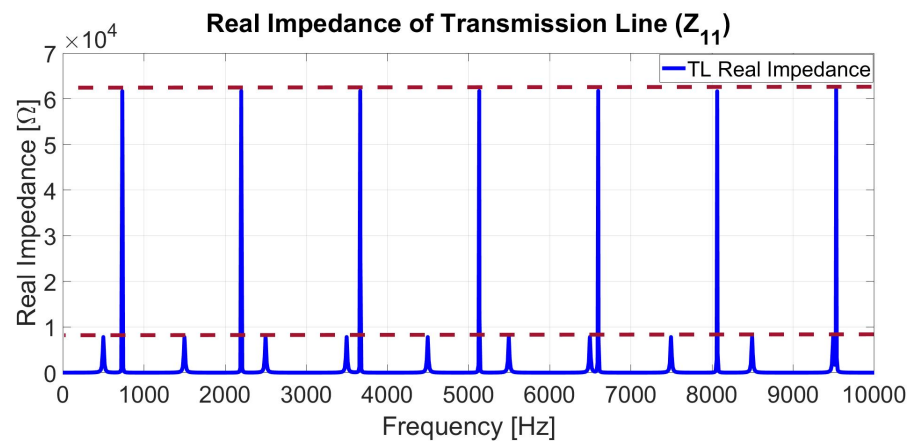
Figure 8. Frequency response measurements of transmission line real impedance.

4.2. Model Parameters Calculation of Z_{11}

Through mathematical derivation and the measured frequency response of transmission line impedance, six equations were obtained with six unknowns. Solving (23), (98), and (99) for L_2 will yield:

$$L_2^2(a) + L_2(b) + c = 0 \tag{100}$$

$$a = 2Z_{R1}\pi^2 + 2\frac{\pi^2\omega_1^2}{\omega_2^2}Z_{R2} \tag{101}$$

$$b = -4L_T\frac{\pi^2\omega_1^2}{\omega_2^2}Z_{R2} \tag{102}$$

$$c = 2L_T^2\frac{\pi^2\omega_1^2}{\omega_2^2}Z_{R2} - \frac{\pi^4}{4\omega_2^2}Z_{R1}R_TZ_{R2} \tag{103}$$

Since Z_{11} at 10^{-6} Hz:

$$Z_{11} = 13.297721647936953 + 0.000001099829278i\,\Omega \tag{104}$$

Then,

$$R_T = 13.297721647936953\Omega \tag{105}$$

$$L_T = 0.175043266078569H \tag{106}$$

where

$$Z_{R1} = 7.815850394108994e + 03\Omega \tag{107}$$

$$Z_{R2} = 6.171053383188052e + 04\Omega \tag{108}$$

At:

$$f_{o1} = 499.55 \text{ Hz} \qquad\qquad f_{o2} = 733.15 \text{ Hz} \tag{109}$$

$$\omega_1 = 2\pi f_{o1} \qquad\qquad \omega_2 = 2\pi f_{o2} \tag{110}$$

By solving the second-order (100), the proposed model parameters of Z_{11} are calculated, see Table 5.

Table 5. Proposed model calculated parameters for Z_{11}.

Transmission Line Parameters	Calculation
R_1	12.070792 [Ω]
L_1	0.108695 [H]
C_1	2.304245 [µF]
R_2	1.226930 [Ω]
L_2	0.066348 [H]
C_2	1.752583 [µF]

By substituting the calculated proposed model parameters from Table 5 in (18), the transmission line measured and the fitted impedance for both real and imaginary of Z_{11} are shown in Figures 9 and 10, respectively.
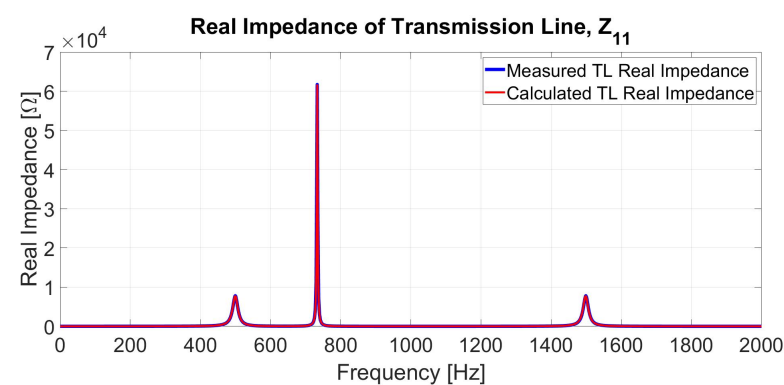
Figure 9. Frequency response measurements and the proposed model calculation of transmission line real impedance (Z_{11}).
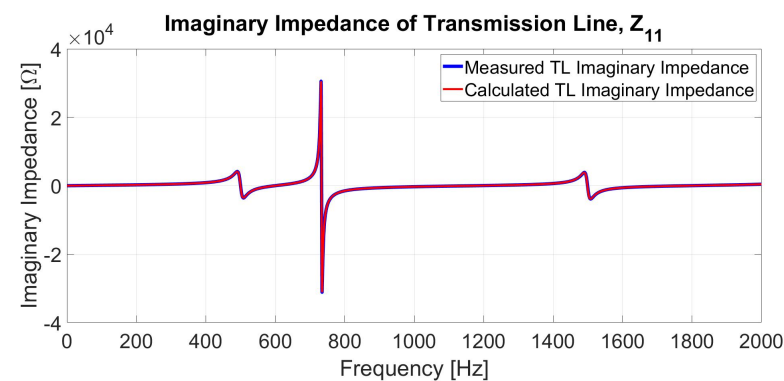
Figure 10. Frequency response measurements and the proposed model calculation of transmission line imaginary impedance (Z_{11}).

4.3. Model Parameters Calculation of Z_{12}

The FRA impedance measurements of the transmission line are obtained in a symmetrical matrix format from RTDS. The impedance matrix of the transmission line at every single measured frequency point is in the form:

$$\begin{bmatrix} Z_{11} & Z_{12} & Z_{13} \\ Z_{21} & Z_{22} & Z_{23} \\ Z_{31} & Z_{32} & Z_{33} \end{bmatrix} \tag{111}$$

where

$$Z_{12} = Z_{21} = Z_{13} = Z_{31} = Z_{23} = Z_{32} \tag{112}$$

$$Z_{11} = Z_{22} = Z_{33} \tag{113}$$

From the mathematical formula derived in the last section, the parameters of Z_{12} can be calculated using the FRA impedance measurements of Z_{12}. Figures 11 and 12 show the FRA of transmission line impedance of Z_{11} and Z_{12} for both real and imaginary part respectively. Therefore, comparing Z_{11} and Z_{12} in Figures 11 and 12 show that at the first resonance, $f_{o1} = 500$ Hz, both the real and imaginary part of Z_{11} and Z_{12} have the same values. In contrast, the second resonance, $f_{o2} = 733$ Hz, both the real and imaginary part of Z_{11} and Z_{12} have a different values with an opposite sign. Therefore, by comparing both Figures 11 and 12, we can derive the impedance equation which describes Z_{12}. Therefore, since

$$Z_{11} = Z_{o1} \times \tanh \gamma_1 l + Z_{o2} \times \tanh \gamma_2 l \tag{114}$$

Which is simplified to

$$Z_{11} = Z1 + Z2 \tag{115}$$

Then for Z_{12},

$$Z_{12} = Z3 - Z4 \tag{116}$$

and since both of Z_{11} and Z_{12} have the same real and imaginary values for the first resonance f_{o1} then,
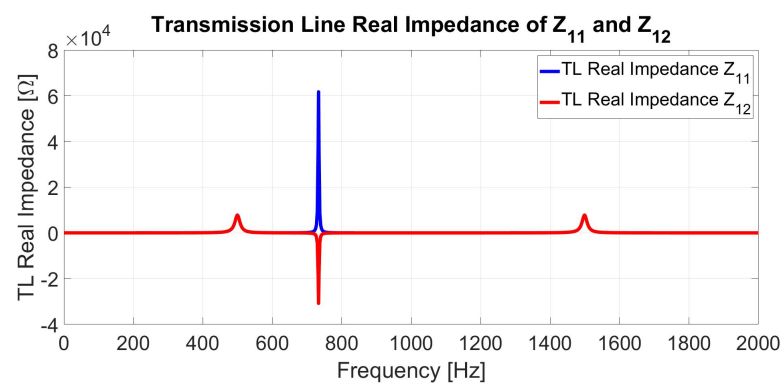
$$Z3 = Z1 \tag{117}$$

Figure 11. Frequency response measurements of transmission line real impedance (Z_{11} and Z_{12}).
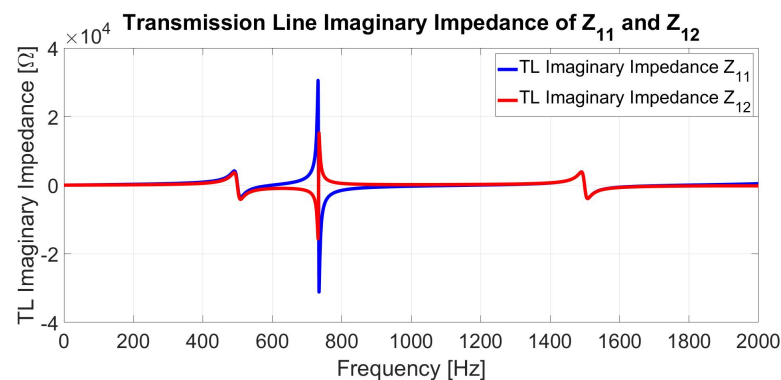

Figure 12. Frequency response measurements of transmission line imaginary impedance (Z_{11} and Z_{12}).

Therefore, to obtain the parameters of Z_{12}, the Equations (23) must change to:

$$R_T = R_3 - R_4 \qquad\qquad L_T = L_3 - L_4 \tag{118}$$

Using Equations (98), (99) and (118), L_4 can be calculated:

$$L_4^2(a) + L_4(b) + c = 0 \tag{119}$$

$$a = 2Z_{R3}\pi^2 - 2\frac{\pi^2\omega_3^2}{\omega_4^2}Z_{R4} \tag{120}$$

$$b = -4L_T\frac{\pi^2\omega_3^2}{\omega_4^2}Z_{R4} \tag{121}$$

$$c = -2L_T^2\frac{\pi^2\omega_3^2}{\omega_4^2}Z_{R4} + \frac{\pi^4}{4\omega_4^4}Z_{R3}R_TZ_{R4} \tag{122}$$

Since Z_{12} at 1×10^{-6} Hz:

$$Z_{12} = 11.443021182700990 + 0.000000472154060i\,\Omega \tag{123}$$

Then,

$$R_T = 11.443021182700990\,\Omega \tag{124}$$

$$L_T = 0.075145652597228H \tag{125}$$

$$Z_{R3} = 7.810237767027844e + 03\,\Omega \tag{126}$$

$$Z_{R4} = 3.084092525461649e + 04\,\Omega \tag{127}$$

$$f_{o3} = 499.55 \text{ Hz} \qquad\qquad f_{o4} = 733.14 \text{ Hz} \tag{128}$$

$$\omega_3 = 2\pi f_{o3} \qquad\qquad \omega_4 = 2\pi f_{o4} \tag{129}$$

By solving the second order equation, the proposed model parameters of Z_{12} can be calculated. Table 6 shows that R_3, L_3, and C_3 have the same values as R_1, L_1, and C_1 of Z_{11} from Table 5. Therefore, the calculation carried out to find all the parameters was not necessary, but shows that the values of $Z1$ and $Z3$ are equal in (117). Since the values of R_3, L_3, and C_3 are already obtained in Table 5, then Equations (98), (99) and (118) can be used to calculate R_4, L_4, and C_4 for Z_{12}.

Table 6. Proposed model calculated parameters for Z_{12}, Z_{13}, and Z_{23}.

Transmission Line Parameters	Calculation
R_3	12.068966 [Ω]
L_3	0.1086480 [H]
C_3	2.3052476 [μF]
R_4	0.6259449 [Ω]
L_4	0.0335024 [H]
C_4	3.4709012 [μF]

Moreover, another method to obtain the line parameters for $Z2$ is by taking the ratio of Z_{R2} to Z_{R4}. Therefore, let

$$\alpha = \frac{Z_{R2}}{Z_{R4}} = 2.000930040924867 \approx 2 \tag{130}$$

To maintain the same resonance at f_{o2}, and reduce the value of Z_{R2} from (108) by α, then

$$L_4 = \frac{L_2}{\alpha} \qquad\qquad C_4 = C_2\alpha \qquad\qquad R_4 = \frac{R_2}{\alpha} \tag{131}$$

Once these sets of Equations (131) are met, then the resonance frequency will remain the same (98), while the magnitude of Z_{R2} will drop to match the measured value of Z_{12} (99). Comparing the vales of R_4, L_4, and C_4 from Table 6 with the values of R_2, L_2, and C_2

from Table 5 shows that the values of R_4 and L_4 were halved while the value of C_4 was doubled. Therefore, the impedance of Z_{12} (116), can be written using the parameters of Z_{11}:
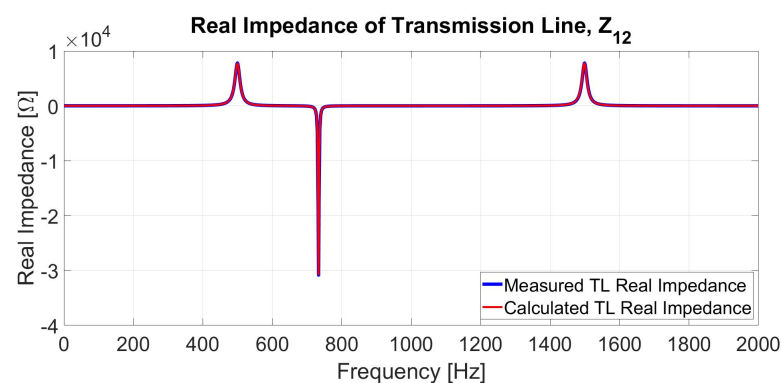
$$Z_{12} = Z3 - Z4 = Z1 - \frac{Z2}{\alpha} \tag{132}$$

From the calculated model parameters in Table 6, and by using equation:

$$Z_{12} = \sqrt{\frac{R_3 + j\omega L_3}{G_3 + j\omega C_3}} \times \tanh\sqrt{(R_3 + j\omega L_3)(G_3 + j\omega C_3)} - \sqrt{\frac{R_4 + j\omega L_4}{G_4 + j\omega C_4}} \times \tanh\sqrt{(R_4 + j\omega L_4)(G_4 + j\omega C_4)} \tag{133}$$

where ($G_3 = G_4 = G_1$).

The real and imaginary impedance of the measured and the fitted impedance of Z_{12} are shown in Figures 13 and 14, respectively.

Figure 13. Frequency response measurements and the proposed model calculation of transmission line real impedance (Z_{12}).
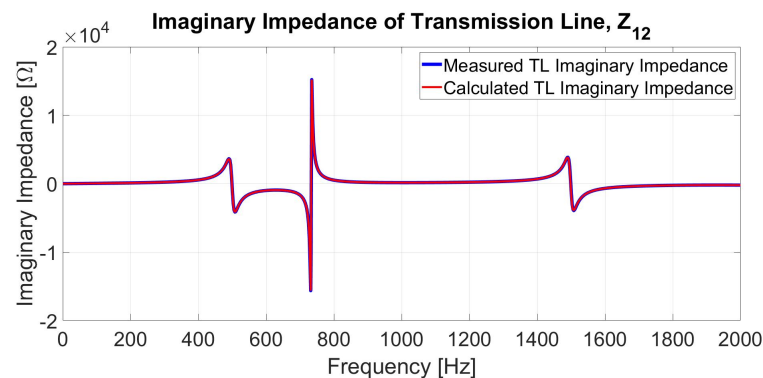
Figure 14. Frequency response measurements and the proposed model calculation of transmission line imaginary impedance (Z_{12}).

5. Developed Algorithm for an Accurate Fitting

An algorithm is developed to minimize the error between the measured impedance frequency response and the proposed model. The calculation of the proposed model parameters has some initial approximation. Therefore, the presented algorithm uses the calculated parameters of the proposed model as initial values to obtain a better fit of the MTL impedance. The proposed algorithm is shown in Algorithm 1.

The parameters of the proposed model which fit the measured impedance of Z_{11}, Z_{12}, and Z_{23} more accurately are shown in Tables 7, 8 and 9, respectively.

Tables 7–9 show the error between the calculated and the fitted parameters of the proposed model for Z_{11}, Z_{12}, and Z_{23}. Even though some approximation was made in solving the transmission line impedance equations, the maximum error between the fitted

and the calculated parameters is within 1%. The parameters obtained from the algorithm are shown in Tables 7–9, which are used to fit the impedance of the MTLs in a 1 MHz range.

Algorithm 1 Developed Algorithm for an accurate model.

Require: The calculated initial values $(R_1, L_1, C_1, R_2, L_2, and\ C_2)$
  Calculate the Error and $\sum$ Error
  while Error$<$x $||$ $\sum$ Error is +ve $>$ (x1) $||$ $\sum$ Error is -ve $<$ (-x1) **do**
    while Error$<$x **do**
      Calculate the Error
      Calculate dL_1, dC_1, dL_2, and dC_2
      Calculate the new error after changing $L_1 = L_1 + dL_1$
      Calculate the new error after changing $C_1 = C_1 + dC_1$
      Calculate the new error after changing $L_2 = L_2 + dL_2$
      Calculate the new error after changing $C_2 = C_2 + dC_2$
      Change the parameters which give the minimum error
    end while
    if $\sum$ Error is +ve $>$ (x1) **then**
      $R_1 = R_1 - dR_1$
      $R_2 = R_2 + dR_2$
    else if $\sum$ Error is -ve $<$ (-x1) **then**
      $R_1 = R_1 + dR_1$
      $R_2 = R_2 - dR_2$
    end if
  end while

Table 7. The calculated and fitted parameters of the proposed model for Z_{11}.

TL Parameters	Calculated	Fitted	Error %
R_1	12.070792 [Ω]	12.06 [Ω]	0.0895
L_1	0.108695 [H]	0.108547 [H]	0.1371
C_1	2.304245 [μF]	2.305941 [μF]	0.0735
R_2	1.226930 [Ω]	1.237722 [Ω]	0.8719
L_2	0.066348 [H]	0.066593 [H]	0.3678
C_2	1.752583 [μF]	1.746129 [μF]	0.3696

Table 8. The calculated and fitted parameters of the proposed model for Z_{12}.

TL Parameters	Calculated	Fitted	Error %
R_3	12.068966 [Ω]	12.06 [Ω]	0.0743
L_3	0.1086480 [H]	0.108546 [H]	0.0944
C_3	2.3052476 [μF]	2.305959 [μF]	0.0309
R_4	0.6259449 [Ω]	0.618861 [Ω]	1.1447
L_4	0.0335024 [H]	0.033297 [H]	0.6179
C_4	3.4709012 [μF]	3.492238 [μF]	0.6110

Table 9. The calculated and fitted parameters of the proposed model for Z_{23}.

TL Parameters	Calculated	Fitted	Error %
R_5	12.068966 [Ω]	12.06 [Ω]	0.0743
L_5	0.1086480 [H]	0.108546 [H]	0.0944
C_5	2.3052476 [μF]	2.305959 [μF]	0.0309
R_6	0.6259449 [Ω]	0.618861 [Ω]	1.1447
L_6	0.0335024 [H]	0.033296 [H]	0.6191
C_6	3.4709012 [μF]	3.492282 [μF]	0.6122

The parameters of Z_{23} are slightly different from Z_{12} and Z_{13}. This is due to the difference in the impedance measurement obtained from RTDS. Therefore, to have a more accurate fit for the proposed model, the algorithm is used for Z_{23} as well. Comparing the Tables 8 and 9 shows that the difference between the parameters of Z_{23} and Z_{12} is small. Figure 15 shows the implementation procedure of the proposed model.
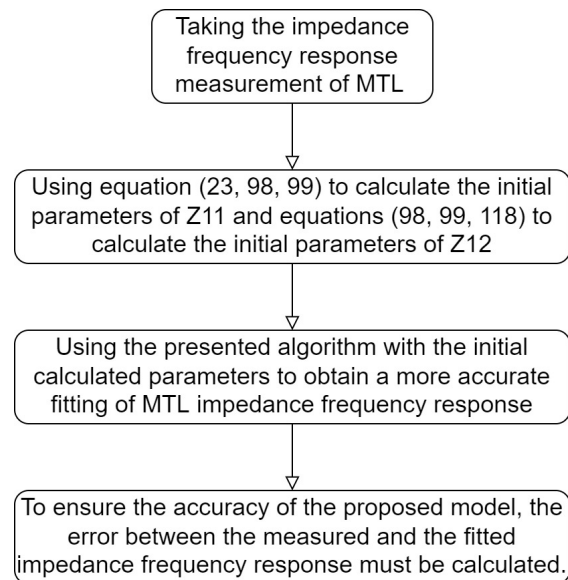

Figure 15. Implementation procedure of the proposed model.

6. Simulation Results

To ensure the accuracy of the proposed model, a well-known and developed fitted method to fit MTL impedance is used—VF. VF is a robust method of rational function approximation. VF is a general methodology to fit the measured or simulated transient frequency response of electric equipment or an n-port network. VF has been used to model the transient behavior of transmission lines and underground cables. The rational function approximation of VF is given by [2]:

$$f(s) = \sum_{n=1}^{N} \frac{c_n}{s - a_n} + d + s.h \tag{134}$$

where, C_n: Residues, a_n: poles, d and h : real numbers, and n: the number of approximation. Therefore, to have a better fit of the measured data, the number of approximation (n) must have a higher value.

The proposed model uses the set of equations derived from the frequency response measurement of MTL impedance based on the analytical impedance equation. Equation (18) and the parameters obtain from the fitting algorithm in Table 7 are used to calculate Z_{11}, Z_{22}, and Z_{33}. For Z_{12}, Z_{21}, Z_{13}, Z_{31}, Z_{23}, and Z_{32} Equation (133), the parameters in Tables 8 and 9 are used for Z_{12} and Z_{23}, respectively.
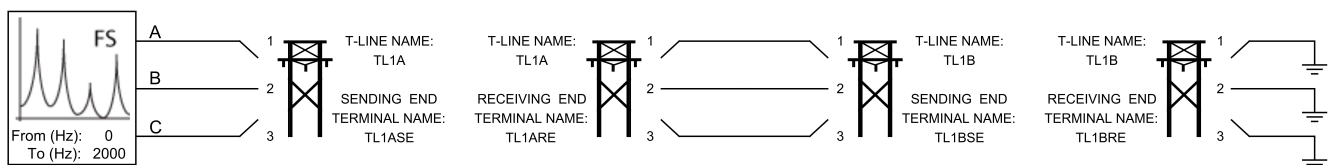
The impedance fitting of the transmission line for different frequency ranges will be shown for the presented model and VF method. For the proposed analytical model, the parameters and the equations will be fixed under different frequency ranges. In addition, the error between the measured and the fitted impedance for both models will be presented. The measurement of the transmission line impedance was carried out on RTDS. The used model and data in the simulated transmission line are shown in Table 10. The RTDS circuit line diagram is shown in Figure 16. Table 10 shows the parameters of the entire transmission line shown in Figure 16. Therefore, each section of the transmission line shown in Figure 16 is 50 km long.

Table 10. Transmission line Bergeron model parameters.

Model	Bergeron (RLC Data Entry)
Line Length	100 [Km]
Transposition	Ideally Transposed
Frequency	60 [Hz]
Ground Resistivity	100 [Ω-m]
Number of Phases	3
Positive Sequence Series Resistance	0.018547 [Ω/Km]
Positive Sequence Series Ind. Reactance	0.37661 [Ω/Km]
Positive Sequence Shunt Cap. Reactance	0.22789 [Meaga$\Omega \times$Km]
Zero Sequence Series Resistance	0.3618376[Ω/Km]
Zero Sequence Series Ind. Reactance	1.227747 [Ω/Km]
Zero Sequence Shunt Cap. Reactance	0.34513 [Meaga$\Omega \times$Km]

Figure 16. RTDS circuit Line Diagram of FRA measurements.

6.1. Case 1: MTL Impedance Fitting for up to 10 kHz Frequency Range

In this case, the tested frequency range is 1^{-6} to 10 kHz. The number of approximations used for the VF is set to 50 (n = 50). Figures 17 and 18 show the magnitude and the angle of the proposed model and the measurement of the transmission line impedance, respectively. The green line in Figure 17 shows the error between the measured and fitted impedance of the three-phase transmission line using the proposed model with a maximum error of 0.1111%.

Figures 19 and 20 show the magnitude and the angle of the VF method and the measurement of the transmission line impedance, respectively. The green lines in Figure 19 show the error between the measured and fitted impedance of the three-phase transmission line using the VF method with a maximum error of 0.0222%.

6.2. Case 2: MTL Impedance Fitting for up to 100 kHz Frequency Range

In this case, the tested frequency range is up to 100 kHz. The number of approximations for the VF is set to 750 (n = 750). Figures 21 and 22 show the magnitude and the angle of the proposed model and the measurement of the transmission line impedance, respectively. The green lines in Figure 21 show the error between the measured and fitted impedance of the three-phase transmission line using the proposed model with a maximum error of 0.1309%.
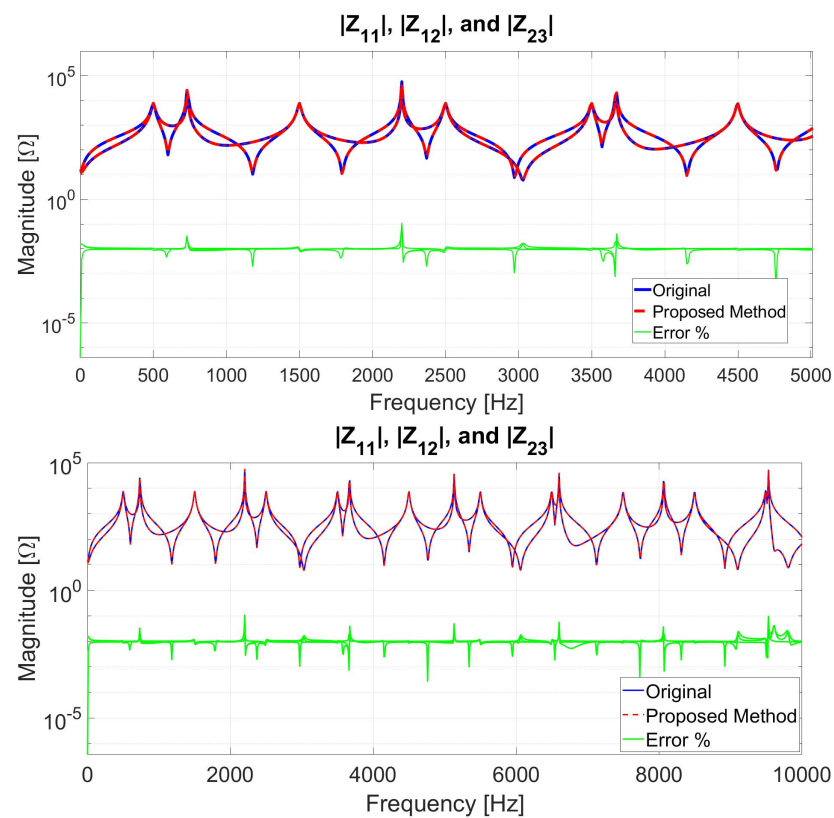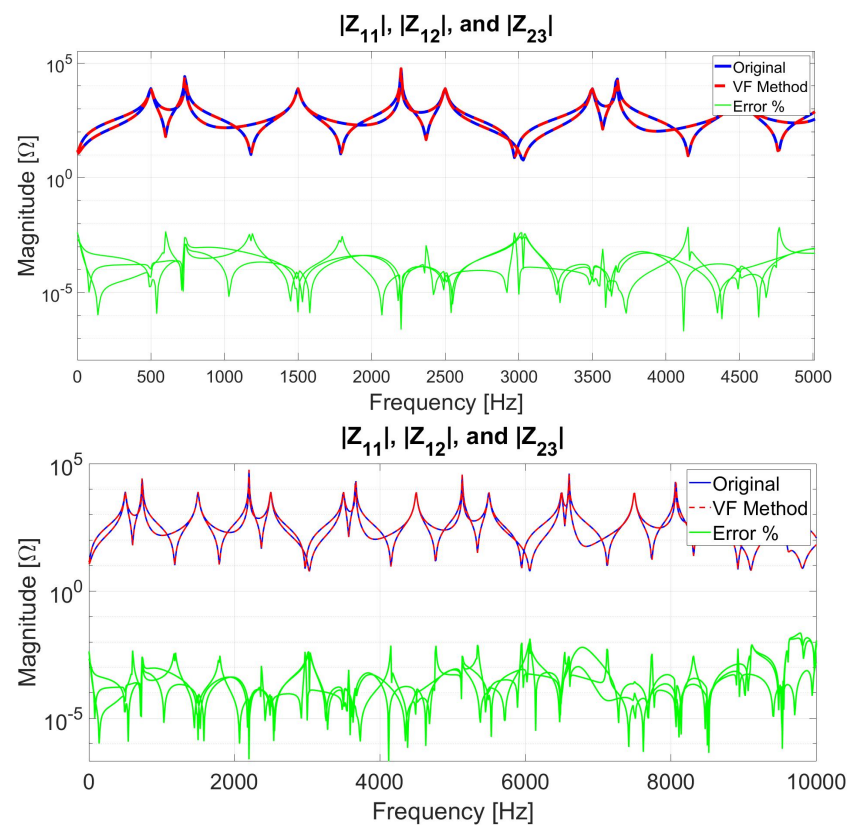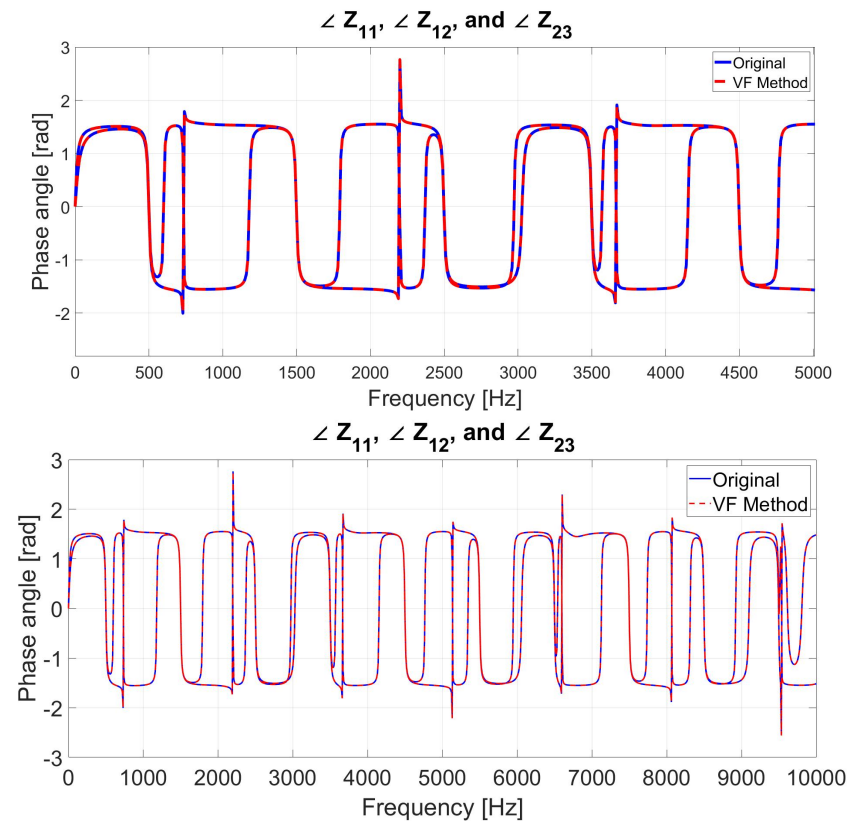
Figure 17. The magnitude of the measured and fitted impedance using the proposed model, $|Z_{11}|$, $|Z_{12}|$, and $|Z_{23}|$.
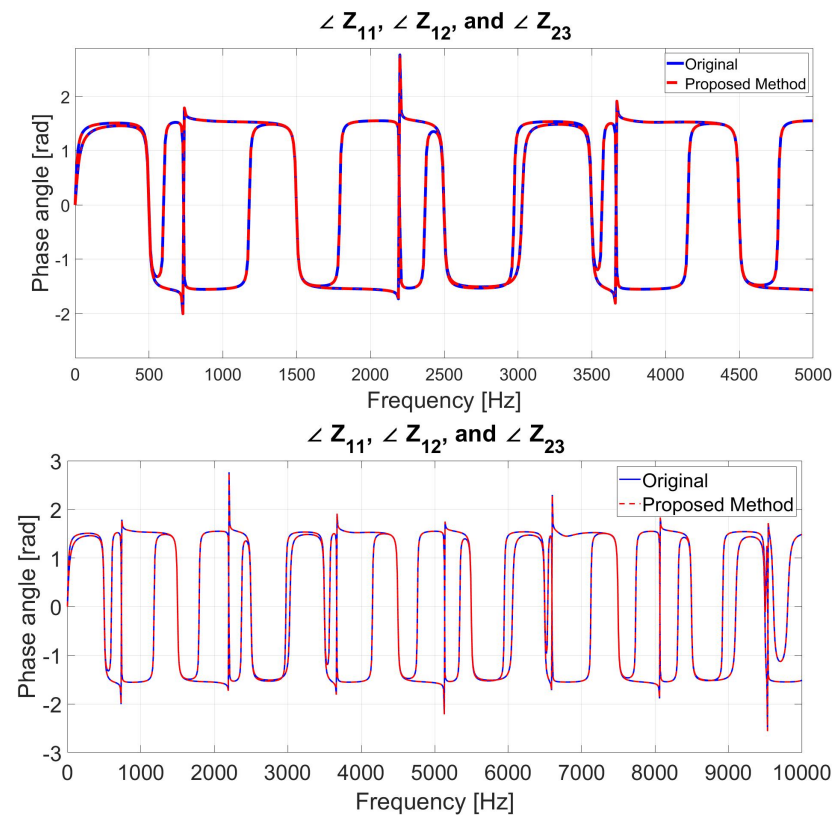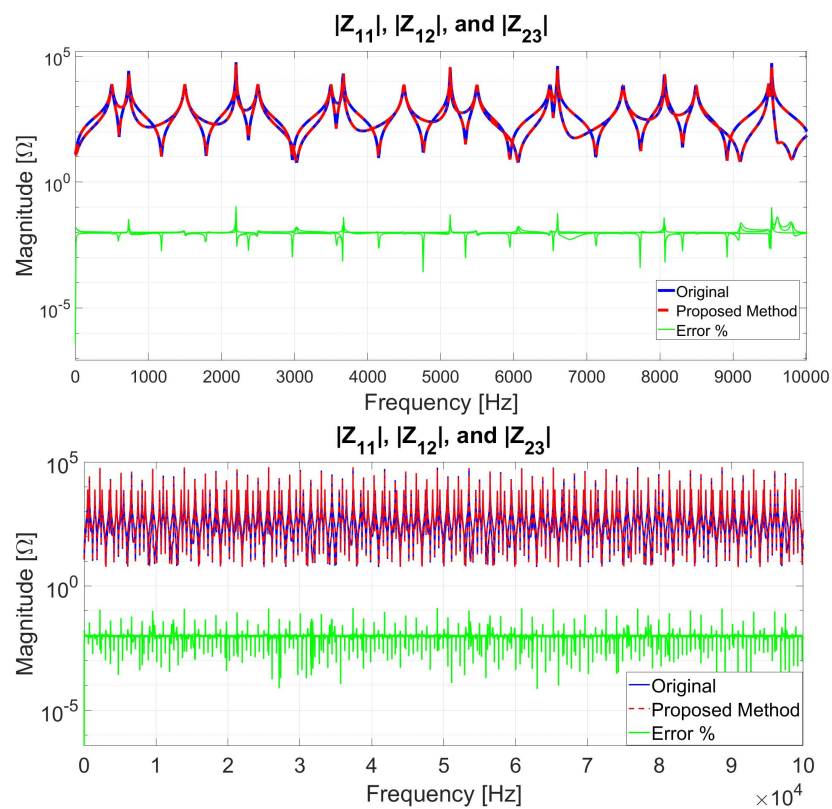

Figure 18. The angle of the measured and fitted impedance using the proposed model impedance, $\angle Z_{11}$, $\angle Z_{12}$, and $\angle Z_{23}$.
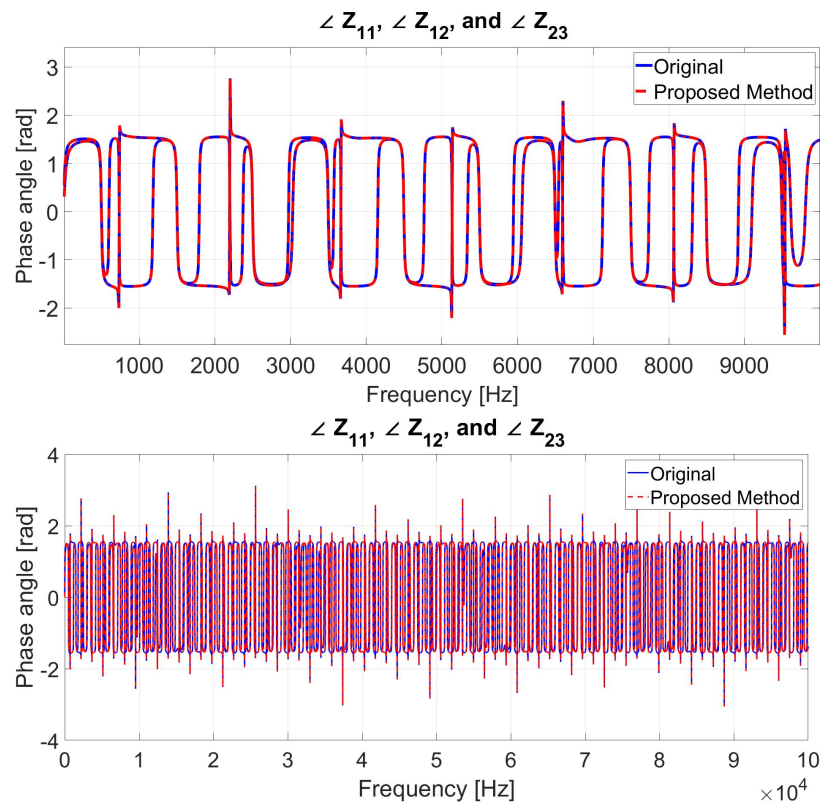
Figure 19. The magnitude of the measured and fitted impedance using VF, $|Z_{11}|$, $|Z_{12}|$, and $|Z_{23}|$.

Figure 20. The angle of the measured and fitted impedance using VF , $\angle Z_{11}$, $\angle Z_{12}$, and $\angle Z_{23}$.
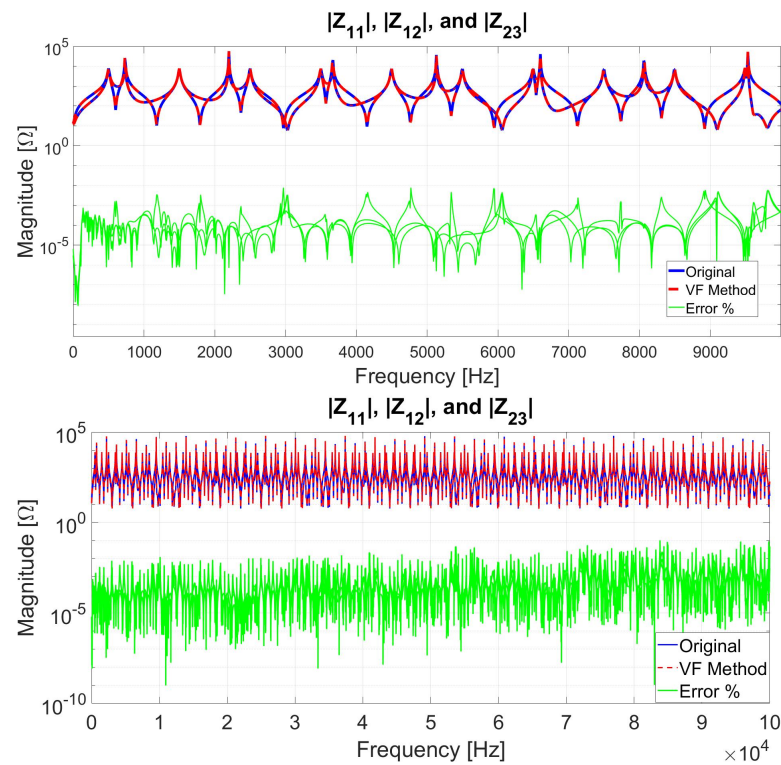
Figure 21. The magnitude of the measured and fitted impedance using the proposed model, $|Z_{11}|$, $|Z_{12}|$, and $|Z_{23}|$.

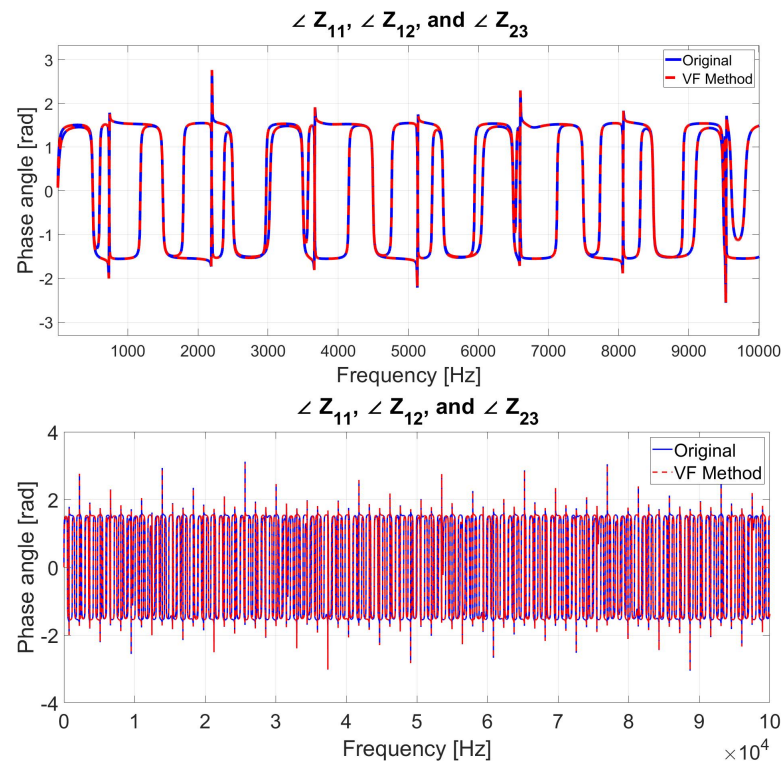

Figure 22. The Angle of the measured and fitted impedance using the proposed model, $\angle Z_{11}$, $\angle Z_{12}$, and $\angle Z_{23}$.

Figures 23 and 24 show the magnitude and the angle of the VF method and the measurement of the transmission line impedance, respectively. The green lines in Figure 23 show the error between the measured and fitted impedance of the three-phase transmission line using the VF method with a maximum error of 0.1039%.
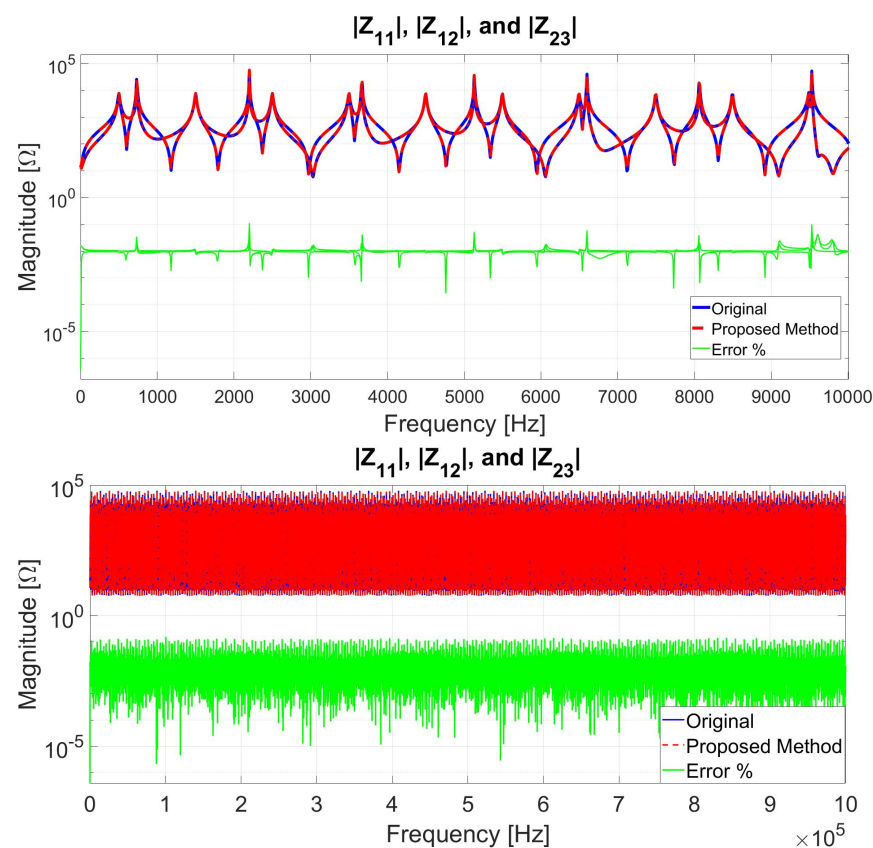

Figure 23. The magnitude of the measured and fitted impedance using VF, $|Z_{11}|$, $|Z_{12}|$, and $|Z_{23}|$.

Figure 24. The angle of the measured and fitted impedance using VF , $\angle Z_{11}$, $\angle Z_{12}$, and $\angle Z_{23}$.

6.3. Case 3: MTL Impedance Fitting for up to 1 MHz Frequency Range

In this case, the tested frequency range is up to 1 MHz. Assuming a linear relationship between the frequency range and the number of approximation (n) from the previous cases, then the number of approximations required to fit the impedance curve using VF for the 1 MHz range is 11,250. Simulating this high number of approximations is highly computational costly. Therefore, for cases 3 and 4, only the proposed model results will be shown. Figures 25 and 26 show the magnitude and the angle of the proposed model and the measurement of the transmission line impedance, respectively. The green lines in Figure 25 show the error between the measured and fitted impedance of the three-phase transmission line using the proposed model with a maximum error of 0.1530%.
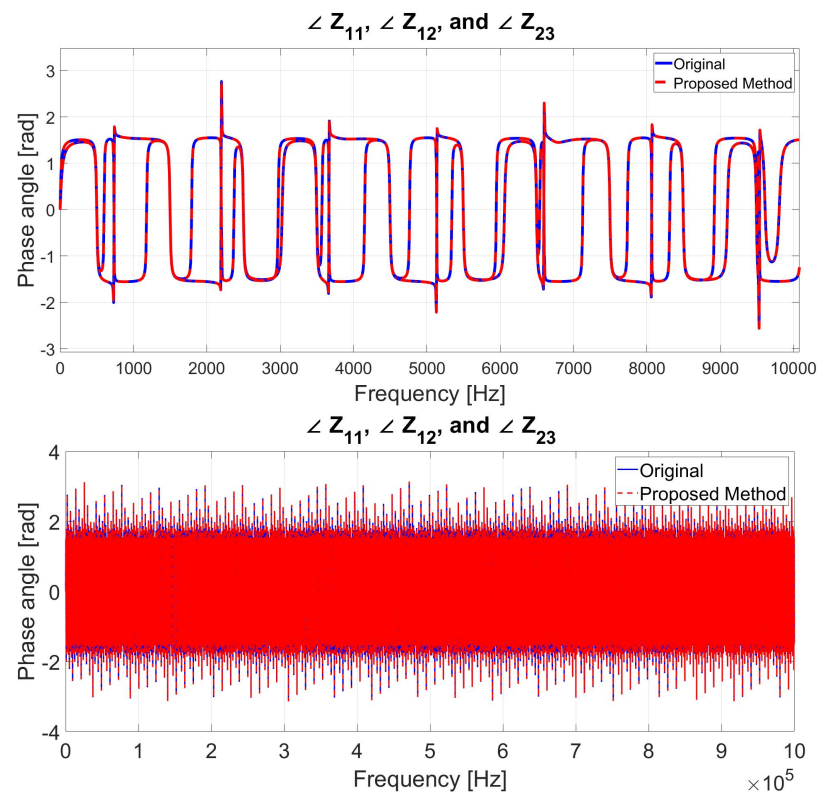

Figure 25. The magnitude of the measured and fitted impedance using the proposed model, $|Z_{11}|$, $|Z_{12}|$, and $|Z_{23}|$.

6.4. Case 4: Changing the Transmission Line Length for 1 MHz Frequency Range

Since the proposed model is based on the analytical impedance equation of a finite transmission line, then the model must correlate to the transmission line length. Therefore, changing the length of the line will not increase the error level between the measured and calculated transmission line impedance. The new length of the simulated transmission line is (150 km). Since the added length of the line is half of the original length, then all the parameters of Z_{11}, Z_{12}, and Z_{23} in Tables 7–9 are multiplied by (1.5). Figures 27 and 28 show the magnitude and the angle of the proposed model and the measurement of the transmission line impedance, respectively. The green lines in Figure 27 show the error between the measured and fitted impedance of the three-phase transmission line using the proposed model with a maximum error of 0.1660%.
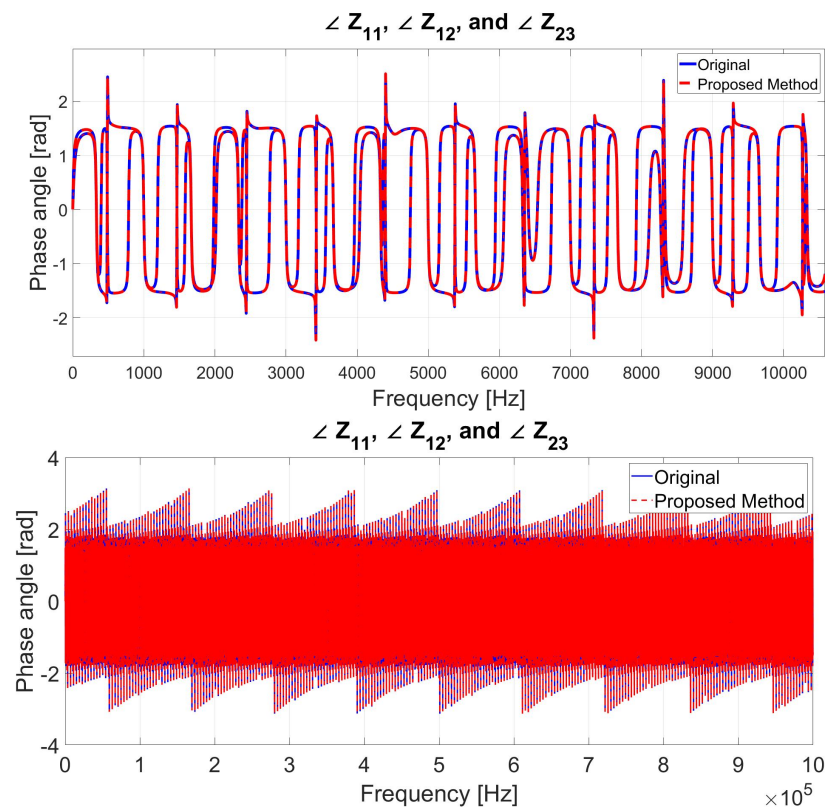
Figure 26. The angle of the measured and fitted impedance using the proposed model, $\angle Z_{11}$, $\angle Z_{12}$, and $\angle Z_{23}$.
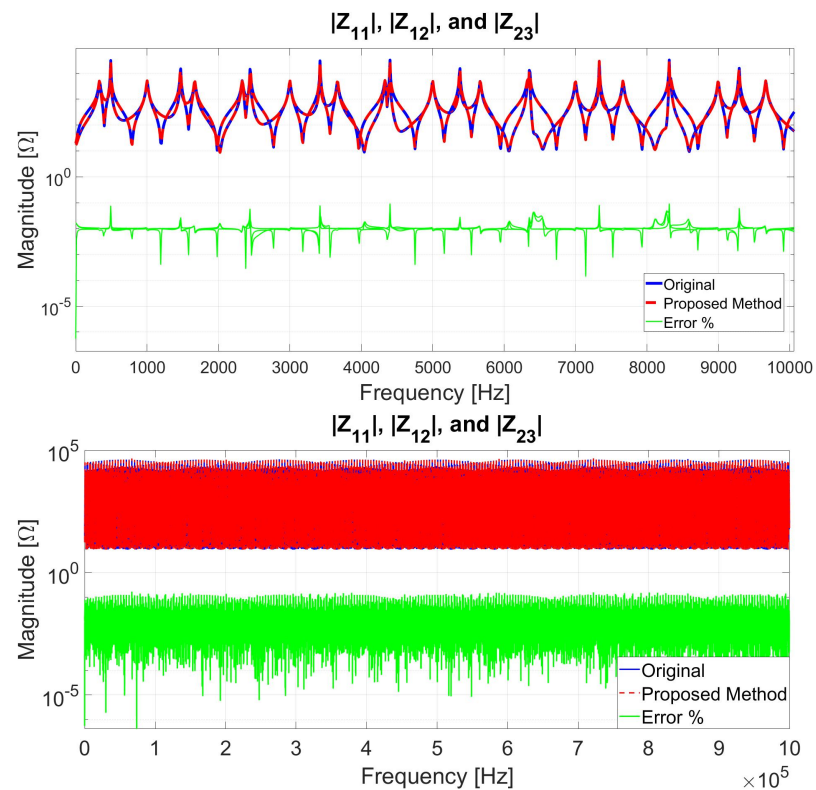
Figure 27. The magnitude of the measured and fitted impedance using the proposed model, $|Z_{11}|$, $|Z_{12}|$, and $|Z_{23}|$.

Figure 28. The angle of the measured and fitted impedance using the proposed model, $\angle Z_{11}$, $\angle Z_{12}$, and $\angle Z_{23}$.

6.5. Computational Time Comparison between the Proposed Method and VF

In this section, the computational time comparison between the proposed method and VF is presented. The fitted impedance of MTL using the VF method was not obtained due to the high computational power requirement for the 1 MHz range. Therefore, the conducted comparison is under the assumption of a linear relationship between the measured time for a lower approximation number (N = 3000) of VF and the required approximation number to fit the impedance curve (N = 11,250). Table 11 presents the computer specifications that have been used to fit the MTL impedance. The maximum number of approximations for VF method that could be fitted using the computer specifications is 3000. Therefore, the VF method required higher computation power to obtain the fitted model. Thus, Table 12 shows the approximation computational time for VF and the exact computational time of the proposed method.

Table 11. The computer specifications.

Computer	Specs
RAM	32 GB, 3200 MHz
CPU	i7-11700F
Operating system	Windows 11

Table 12. Computational time.

Method	Computational Time [S]
VF	24,663.37
Proposed Model	516.75

6.6. Comparison between VF and the Proposed Method

VF method is capable of fitting the transmission line impedance to a very high degree of accuracy. On the other hand, it is required high computational power to develop the model, as shown in the previous cases. In contrast, the proposed model uses a set of constant parameters that are calculated from the impedance frequency response. Therefore, the proposed model does not require a high computational requirement to calculate the model parameters, see Table 13. In addition, the proposed model is based on the impedance equation of a finite transmission line. Thus, the proposed model is a function of transmission line length. However, the VF method is based on the rational function approximation, which is not a function in transmission line length.

Table 13. Comparison between VF and the proposed model.

Frequency [kHz]	Number of Parameters		Computational Power	
	Vector Fitting	Proposed Model	Vector Fitting	Proposed Model
10	50	24	Low	Low
100	750	24	Medium	Low
1000	NA	24	High	Low

Moreover, the VF method required retaking the frequency response impedance measurements in case the frequency range is changed and developing a new model for MTL, see cases 1, 2. The proposed model uses the same equations and the same parameters for a wide range of frequencies, see cases 1, 2, and 3.

7. Features of the Proposed Method

Many different fitting methods have the capability of fitting a set of data to a very high degree of accuracy with minimum error. The fitting is achieved through a set of mathematical equations which may not be correlated to the fitted data. In addition, if the sampling number of the fitted data is small, then the obtained fitted curve, even though fitted to a very high degree, will not give accurate values of the data. For example, Figure 29 shows two different sampling rates of a transmission line impedance (200 and 200 k). This problem manifests when taking the frequency response for a high-frequency range while being limited by a set of the sampling rate. Due to the low sampling rate of the data, the fitted curve does not reflect the correct values.
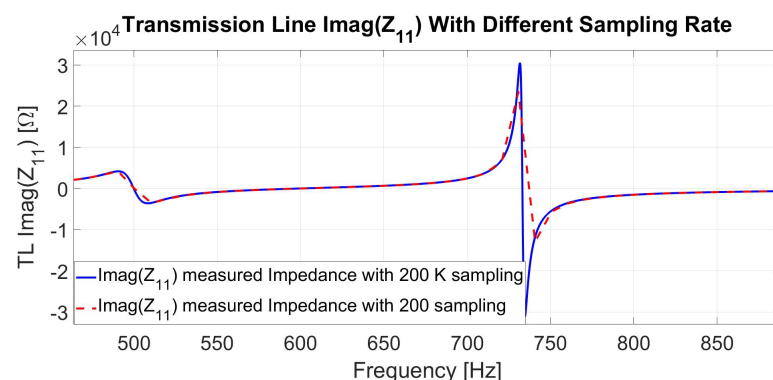
Figure 29. Frequency response measurement of the transmission line imaginary impedance (Z_{11}) with different sampling rates.

In contrast, using the analytical impedance equation to describe the impedance of the transmission line, even with a reduction of sampling rates, will result in a better representation of a transmission line impedance.

In addition, the proposed method is based on finite transmission line impedance, which is a function of the transmission line length. Therefore, changing the length of

the transmission line will not require any changes in the model, as shown in case 4, unlike different fitting methods, which required retaking the frequency response of the transmission line and generating new parameters for a mathematical function.

Moreover, curve fitting methods require a high number of approximations to fit the impedance curve of the transmission line for a high-frequency range, which in turn reflects in the high number of terms the mathematical function required to fit the curve. Moreover, the higher number of approximations will require more computational power to fit the impedance curve. In contrast, the proposed analytical solution has a constant set of terms and parameters which will not change with the frequency range, see cases 1, 2, and 3.

8. Conclusions

In this paper, a novel fitting method of MTL based on the analytical impedance equation of a transmission line using the impedance frequency response measurement is presented. The impedance frequency response of MTL is measured using a RTDS. Moreover, the parameters of the proposed model are calculated using derived resonance equations and the impedance frequency response measurement. In addition, an algorithm is developed to further fit the proposed model to the impedance frequency response measurement of MTL. The error between the calculated model parameters using the derived resonance equations and the fitted ones is within 1%. The proposed fitting model is a function of the transmission line length, since it is based on the analytical impedance equation of a finite transmission line. Therefore, changing the transmission line length will not require retaking the impedance frequency response of MTL, as shown in case 4. Furthermore, the proposed model uses a fixed set of equations (Z_{11}, Z_{12}, and Z_{23}) and constant parameters (R, L, C, and G) to fit the impedance frequency response for a wide range of frequencies, as shown in cases 1, 2, and 3.

Author Contributions: Conceptualization, H.A. and M.A.; Formal analysis, H.A., M.A. and M.K.; Funding acquisition, M.A.; Software, M.K.; Investigation, H.A.; Methodology, H.A., M.A. and M.K.; Supervision, M.A. and M.K.; Validation, H.A.; Visualization, M.K.; Writing—original draft, H.A.; Writing—review and editing, M.A. and M.K. All authors have read and agreed to the published version of the manuscript.

Conflicts of Interest: The authors declares that there is no conflict of interest regarding the publication of this paper.

References

1. Gustavsen, B.; Semlyen, A. Rational approximation of frequency domain responses by vector fitting. *IEEE Trans. Power Deliv.* **1999**, *14*, 1052–1061. [CrossRef]
2. Gustavsen, B.; Semlyen, A. Simulation of transmission line transients using vector fitting and modal decomposition. *IEEE Trans. Power Deliv.* **1998**, *13*, 605–614. [CrossRef]
3. Gustavsen, B.; Semlyen, A. Combined phase and modal domain calculation of transmission line transients based on vector fitting. *IEEE Trans. Power Deliv.* **1998**, *13*, 596–604. [CrossRef]
4. Morched, A.; Gustavsen, B.; Tartibi, M. A universal model for accurate calculation of electromagnetic transients on overhead lines and underground cables. *IEEE Trans. Power Deliv.* **1999**, *14*, 1032–1038. [CrossRef]

5. Gustavsen, B. Frequency-dependent transmission line modeling utilizing transposed conditions. *IEEE Trans. Power Deliv.* **2002**, *17*, 834–839. [CrossRef]
6. Ming, T.; Jianyang, S.; Jianzhao, G.; Hongjie, L.; Wei, Z.; Deliang, L. Time-Domain Modeling and Simulation of Partial Discharge on Medium-Voltage Cables by Vector Fitting Method. *IEEE Trans. Magn.* **2014**, *50*, 993–996. [CrossRef]
7. Gustavsen, B.; Heitz, C. Fast Realization of the Modal Vector Fitting Method for Rational Modeling with Accurate Representation of Small Eigenvalues. *IEEE Trans. Power Deliv.* **2009**, *24*, 1396–1405. [CrossRef]
8. Kocar, I.; Mahseredjian, J. Accurate Frequency Dependent Cable Model for Electromagnetic Transients. *IEEE Trans. Power Deliv.* **2016**, *31*, 1281–1288. [CrossRef]
9. Ramirez, A.; Iravani, R. Enhanced Fitting to Obtain an Accurate DC Response of Transmission Lines in the Analysis of Electromagnetic Transients. *IEEE Trans. Power Deliv.* **2014**, *29*, 2614–2621. [CrossRef]
10. Cervantes, M.; Kocar, I.; Mahseredjian, J.; Ramirez, A. Partitioned Fitting and DC Correction for the Simulation of Electromagnetic Transients in Transmission Lines/Cables. *IEEE Trans. Power Deliv.* **2018**, *33*, 3246–3248. [CrossRef]
11. Gunawardana, M.; Kordi, B. Time-Domain Modeling of Transmission Line Crossing Using Electromagnetic Scattering Theory. *IEEE Trans. Power Deliv.* **2020**, *35*, 1020–1027. [CrossRef]
12. Oh, K.S. Accurate transient simulation of transmission lines with the skin effect. *IEEE Trans. Comput.-Aided Des. Integr. Circuits Syst.* **2000**, *19*, 389–396. [CrossRef]
13. Liu, X.; Cui, X.; Qi, L. Time-Domain Finite-Element Method for the Transient Response of Multiconductor Transmission Lines Excited by an Electromagnetic Field. *IEEE Trans. Electromagn. Compat.* **2011**, *53*, 462–474. [CrossRef]
14. Asghari, B.; Dinavahi, V. Real-Time Nonlinear Transient Simulation Based on Optimized Transmission Line Modeling. *IEEE Trans. Power Syst.* **2011**, *26*, 699–709. [CrossRef]
15. Ramirez, A.; Semlyen, A.; Iravani, R. Modeling nonuniform transmission lines for time domain simulation of electromagnetic transients. *IEEE Trans. Power Deliv.* **2003**, *18*, 968–974. [CrossRef]
16. Du, Z.; Xie, Y.z.; Dong, N.; Canavero, F.G. A Spice-Compatible Macromodel for Field Coupling to Underground Transmission Lines Based on the Analog Behavioral Modeling. *IEEE Trans. Electromagn. Compat.* **2020**, *62*, 2045–2054. [CrossRef]
17. Ghiasi, S.M.S.; Abedi, M.; Hosseinian, S.H. Mutually Coupled Transmission Line Parameter Estimation and Voltage Profile Calculation Using One Terminal Data Sampling and Virtual Black-Box. *IEEE Access* **2019**, *7*, 106805–106812. [CrossRef]
18. Ye, H.; Strunz, K. Multi-Scale and Frequency-Dependent Modeling of Electric Power Transmission Lines. *IEEE Trans. Power Deliv.* **2018**, *33*, 32–41. [CrossRef]
19. Martí, J.R.; Tavighi, A. Frequency-Dependent Multiconductor Transmission Line Model With Collocated Voltage and Current Propagation. *IEEE Trans. Power Deliv.* **2018**, *33*, 71–81. [CrossRef]
20. Cheng, D.K. *Field And Wave Electromagnetic*; Addison Wesley: Boston, MA, USA, 1983.